Journal of Energy Storage 54 (2022) 105223

Contents lists available at ScienceDirect

Journal of Energy Storage

journal homepage: www.elsevier.com/locate/est

Research Papers

Intermittent power control in wind turbines integrated into a hybrid energy storage system based on a new state-of-charge management algorithm

Mauro Amaro Pinazo, Jose Luis Romeral Martinez

Department of Electronic Engineering, Universitat Politècnica de Catalunya, MCIA Research Center, 08222 Terrassa, Barcelona, Spain

ARTICLE INFO

Keywords:
Battery energy storage systems
Direct-drive permanent magnet synchronous generator
Inertia
Intermittent power
Supercapacitor energy storage systems
Wind turbine

ABSTRACT

Wind technology has developed sustainably in recent decades, becoming the primary source of renewable energy integrated into the power system. The high penetration levels of wind energy involve technical problems because of the intermittent power injected by wind turbines, caused by the variability of wind speed. This means a significant challenge in the operation of power grids reliably. This paper presents the intermittent power control in wind turbines based on direct-drive permanent magnet synchronous generator technology (DD-PMSG) integrating through the DC link a hybrid energy storage system (HESS) composed of lithium-ion electrochemical batteries (BESS) and supercapacitors (SESS), to convert a wind power plant into a dispatchable energy source. To ensure the stable operation of the wind turbine and HESS system, a new algorithm is developed to manage the state-of-charge (SOC) of the HESS to avoid its full charge/discharge. This is achieved by considering the mutual support between the batteries and the supercapacitors. The simulation results illustrate the power variation of the wind turbine integrated to the HESS, with different wind speed profiles and different initial state-of-charge for the BESS and SESS. Furthermore, it is shown how the algorithm manages the state-of-charge of the HESS under both normal and critical operation, demonstrating a good performance during the system operation. In this way, the power output of the wind turbine becomes stable and controllable, even in adverse situations, thanks to the control of the algorithm. Finally, new concepts related to wind turbine inertia and wind turbine rotational speed have been introduced from the point of view of the generator and the grid, which could be useful for electrical studies. The whole dynamic model has been developed in MATLAB/Simulink.

1. Introduction

Wind energy has shown the fastest growth rate compared to other renewable energy sources lately, even with the constraints related to the COVID-19 pandemic and the global economic-political challenges this has implied. By the end of 2020, total global wind energy capacity increased by 14 % compared to 2019 and approached 763 GW [1]. This is double the capacity compared to that installed in 2014. Considering the sustainable growth of wind power and the variability of wind resources, integrating large levels of wind power into power grids addresses many operational and control challenges that hinder reliable system operation [2,3]. Among the most important challenges are power quality problems, frequency and voltage stability, protection, low voltage ride-through capability, electricity market and wind power intermittency [4]. Short-term power fluctuations and medium to long-term wind speed uncertainty affect the reliability and power quality of the power system. The uncertainty is because of the intermittent nature of atmospheric parameters, such as wind speed and direction, temperature, humidity and ambient pressure, making a wind power plant an irregular and uncontrollable power source. Many of the solutions proposed and used to mitigate and smooth the intermittent power of wind power plants are based on integrating different energy storage technologies. Which have become an excellent support for increasing the integration levels of renewable energies, among them wind energy, providing promising solutions for transforming wind power plants into controllable and dispatchable power sources [5,6]. The main barrier to integration is the cost of energy storage systems, which are mainly application-dependent and vary by location and size. Among the different technologies, supercapacitors and flywheels are the lowest cost technologies when more power is required ($/kW), whereas, pumped hydro and compressed air systems are the lowest capital cost technologies when more power is required ($/kWh) [7]. Different techniques are required to smooth the power fluctuations of wind turbines caused by rapid and random changes, mainly because of the stochastic nature of wind speed. Thus, it is necessary to integrate energy storage systems formed by a single technology or in a hybrid way (two or more

E-mail address: mauro.paul.amaro@estudiantat.upc.edu (M. Amaro Pinazo).

https://doi.org/10.1016/j.est.2022.105223
Received 26 April 2022; Received in revised form 22 June 2022; Accepted 24 June 2022
Available online 9 July 2022

technologies) that improve their performance, efficiency, and lifetime [8,9]. Furthermore, an optimal energy management strategy is required to ensure stable system operation. Several studies have been conducted on power intermittency, its impact on the power system and possible mitigation solutions [10].

In [11], a constant power control model for 3.6 MW DFIG wind turbines integrated to an energy storage system composed of supercapacitors connected to the DC link was developed. The paper proposes a two-layer control algorithm, where the first layer handles the control of each wind turbine with its respective SESS, while the second layer establishes and controlling the constant active power of the wind power plant. In [12], an energy management strategy of a flywheel-based energy storage system (FESS) is proposed. The aim of this paper is to smooth the power output of a variable speed wind turbine by demonstrating that the higher the average wind power, the higher the average rotational speed of the flywheel.

Papers [11,12] have used energy storage based on power requirements. A promising solution to power intermittency is the use of a suitable external hybridization of a high-energy density energy storage system and a high-power density energy storage system to achieve more stable power control and increase system lifetime.

According to [13], the authors introduce a model of a 2 MW wind turbine integrated to a HESS composed of a flywheel and electrochemical batteries. The energy management of the HESS is based on the principle of the simultaneous stochastic perturbation stochastic approximation (SPSA). This study showed that the output power fluctuations of the wind turbine were reduced by over 80 % when compared to the output power of the wind turbine without HESS. From another standpoint, in [14] an energy management algorithm of a HESS composed of batteries and supercapacitors connected to a PMSG wind turbine is proposed to inject constant power to the grid. The algorithm is divided into six operation modes, which depend on the state of charge of the BESS and SESS. When the BESS can no longer be charged or discharged, the SESS comes into operation to replace the BESS operation. The pitch control supports constant power control when the BESS and SESS are at the full charge limit. One disadvantage of this algorithm is that, if the BESS and SESS are at the full discharge limit, the system cannot maintain a constant power output. Instead, it will deliver variable power depending on the wind speed. In [15], a new control strategy for batteries and supercapacitors is proposed to keep the state of charge of the supercapacitor away from its limiting capacity. The control adjusts the reference power of the supercapacitors and batteries according to their state of charge and the remaining charge capacity of the supercapacitors. The authors, in [16], present three ways to inject power from a PMSG wind turbine connected to a BESS. In case 1, a constant average power for a wind speed profile during a time window. In case 2, a ramped power that follows the equation of a straight line during a time window. For case 3, a continuous power follows the wind speed profile, without the high-frequency components. Different methods of dispatching wind power are shown, which can be combined or selected as required by the power system.

This work presents the active power control of a 2.5 MW DD-PMSG wind turbine integrated into a hybrid energy storage system (HESS) composed of lithium-ion electrochemical batteries (BESS) and supercapacitors (SESS). The contribution of this work is the proposal and development of a new algorithm to manage the state of charge of the HESS, with the goal of making the wind turbine power constant and controllable. The algorithm contributes to the increase in the operational efficiency and continuity of the system, allowing it to overcome adverse scenarios without generating transients in the power injected into the grid. Critical scenarios are established for states of charge of the BESS and SESS close to the minimum (20 %) and maximum (95 %) limit to show how the system automatically overcomes these scenarios. The algorithm controls the reference power signal of the wind turbine to avoid total charge/discharge of the BESS. Furthermore, it gradually decreases or increases the reference power signal of the SESS to avoid its total charge/discharge with the support of the BESS until it returns again to the normal operation zone. The algorithm has been developed taking into consideration all possible situations that it can encounter, making it a robust and feasible algorithm for real-time applications. The results show that the control algorithm implemented to the wind turbine-HESS system makes the BESS and SESS operate stably, using their maximum operating region. New concepts related to the inertia constant and the wind turbine rotational speed observed from the grid side have been introduced, which can be very useful for electrical studies of future wind farms.

Finally, the mathematical models for the wind turbine, the energy storage system, the control system, and the state-of-charge management algorithm were developed in MATLAB/Simulink (Table 1).

2. Problem statement

The increase in wind power levels in the power grids implies that wind power plants offer new services, such as participating in frequency regulation and even in automatic generation control. Unfortunately, the stochastic characteristic of wind resources causes variations in generation power, which makes it difficult to balance generation and demand in a scenario of high wind power penetration. Fig. 1 illustrates an area where "m" conventional synchronous generators coexist and, in a steady state, the average electrical speed of all of them must be maintained in any part of the system. This is called a synchronous operation. There are also "n" wind turbines that operate at different speeds because of the decoupling that exists due to their electronic interface and "p" electrical loads.

Two types of problems related to power intermittency can be posed. The first problem is based on the imbalance between generation and demand. From Eq. (1) is formulated taking only conventional generation into account. This equation represents the approximate dynamics of an

Table 1
Summary of references regarding power control and smoothing in wind turbines.

Reference	ESS	Generator	Remarks
[11]	SESS	DFIG	Each SESS wind turbine is regulated by a low-layer controller, and all of them are coordinated by a high-layer wind farm supervisory controller. The wind turbine changes its operating point according to demand.
[12]	FESS	PMSG	The energy management is effective for governing the FESS for wind power smoothing. It is found that the higher mean wind power, the higher mean optimal speed of the flywheel.
[13]	BESS-FESS	PMSG	A stochastic power management strategy based on the SPSA algorithm is developed. A smoother power profile is obtained at the grid interface point and, at the same time, a lower solicitation of the battery.
[14]	BESS-SESS	PMSG	An algorithm is developed to manage the energy, which is based on six operation modes according to the state-of-charge of the BESS and SESS. The BESS and SESS operate separately and are supported by the pith angle control.
[15]	BESS-SESS	PMSG	A state-of-charge control strategy is proposed by adjusting the reference power of the supercapacitors to keep it away from its capacity limit to avoid a small voltage giving rise to a large current.
[16]	BESS	PMSG	Three ways of dispatching wind energy are proposed. A constant power output over a period, a ramped power output, and the last one, a continuous power output curve. Moreover, frequency and voltage support are added.

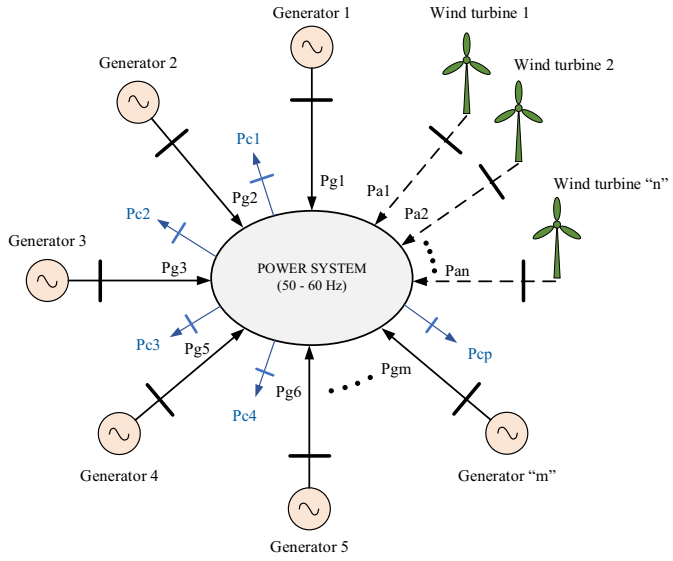

Fig. 1. Simplified diagram of an electrical system in an area.

equivalent machine [13].

$$P_{acc} = \sum_{i=1}^{m} P_{gi} - \sum_{k=1}^{p} P_{ck} \approx 2H_{eq\_sys}\frac{d\omega_s}{dt} \tag{1}$$

where P_{gi} is the power of the conventional synchronous generator "i", P_{ck} is the power of the load "k", P_{acc} is the acceleration power, H_{eq_sys} is the equivalent inertia constant of the system and ω_s is the rotational speed of the generators. The sum of P_{gi} $\left(\sum_{i=1}^{m} P_{gi}\right)$ is a controllable variable while the sum of P_{gi} $\left(\sum_{i=1}^{m} P_{gi}\right)$ is an uncontrollable variable, being its prediction affordable to maintain the balance between generation and demand. Now, the wind generation is added to the dynamics of an equivalent machine through Eq. (2).

$$P_{acc} = \sum_{i=1}^{m} P_{gi} + \sum_{j=1}^{m} P_{aj} - \sum_{k=1}^{p} P_{ck} \approx 2H_{eq\_sys}\frac{d\omega_s}{dt} \tag{2}$$

where P_{aj} is the intermittent power of the wind turbine "j". The sum of P_{aj} $\left(\sum_{j=1}^{m} P_{aj}\right)$ is an uncontrolled variable, whose prediction is complicated since it depends on the wind speed profile. Then, if in Eq. (2) the wind generation increases, there would be two uncontrolled variables $\left(\sum_{k=1}^{p} P_{ck}$ and $\sum_{j=1}^{m} P_{aj}\right)$ which would complicate the balance between generation and demand. The solution to the first problem is to convert the wind turbine power control $\left(\sum_{j=1}^{m} P_{aj}\right)$ into a constant and controllable variable.

The second problem is the decrease in the equivalent inertia constant of the power system. As wind generation increases, the inertia constant of the system decreases, resulting in a greater amplitude of frequency deviations caused by variations between generation and demand. Eq. (3) shows the calculation of the equivalent inertia constant of the system (H_{eq_sys}) comprising conventional synchronous generators and wind turbines.

$$H_{eq\_sys} = \frac{\sum_{i=1}^{m} E_{GS,i} + \sum_{j=1}^{n} E_{AG,j}}{S_T} \tag{3}$$

where $E_{GS,\,i}$ is the kinetic energy of the rotating mass of synchronous generator "i", $E_{AG,\,j}$ is the kinetic energy of the rotating mass of wind turbine "j" and S_T is the total apparent power of the system. Frequency oscillations caused by variations between generation and demand can be damped if the equivalent inertia constant of the system has a high value, i.e., if a large number of conventional synchronous generators are connected to the power grid. However, traditionally in a wind turbine based on PMSG or DFIG technology, it is not possible to use the kinetic energy stored in its large rotating mass. Then, the sum of the kinetic energy stored in the rotor of the n wind turbines is practically zero, as shown in Eq. (4).

$$\sum_{j=1}^{n} E_{AG,j} = 0 \tag{4}$$

As the total installed apparent power (S_T) increases, it causes a decrease in the equivalent inertia constant of the system. The solution to the second problem is to define the inertia constant of the wind turbine based on the control of the wind turbine power as seen from the grid side.

3. Wind energy conversion system model

This section shows a summary of the most important subsystems of the dynamic model of the DD-PMSG wind turbine. Fig. 2 shows the general scheme of the wind turbine connected to an energy storage system so that the active power of the wind turbine is constant and controllable.

3.1. Aerodynamic model

The power available in the wind is converted by the rotor blades into mechanical power by applying Eq. (5) [17].

$$P_m = \frac{1}{2}\rho\pi R^2 C_p(\lambda,\beta)v_w^3 \tag{5}$$

where ρ is the air density, R is the wind turbine blade length, v_w is the wind speed, C_p is the power coefficient, λ is the tip-speed ratio and pitch angle. The power coefficient can be expressed by Eqs. (6) and (7):

$$C_p(\lambda,\beta) = c_1\left[\frac{c_2}{\lambda_i} - c_3\beta - c_4\beta^{c_5} - c_6\right]e^{-\frac{c_7}{\lambda_i}} \tag{6}$$

$$\frac{1}{\lambda_i} = \frac{1}{\lambda + c_8\beta} - \frac{c_9}{\beta^3 + 1} \tag{7}$$

where c_1, c_2, c_3, c_4, c_5, c_6, c_7, c_8, c_9 are the aerodynamic constants that depend on the wind turbine blade design. Fig. 3 shows the surface of the power coefficient $C_p(\lambda,\beta)$ as a function of tip-speed ratio (λ) and pitch angle (β). The wind turbine parameters are shown Table A.1 of Appendix A.

3.2. Mechanical model

A single-mass mechanical drive system considers a rotating disk with a moment of inertia equal to the sum of the individual moments of inertia of the generator and turbine. Since it is a direct-drive wind turbine, it has no gearbox and the entire system rotates at the same speed [18].

$$\left(J_t + J_g\right)\frac{d\Omega_t}{dt} = t_t - t_{em} \tag{8}$$

where J_t, J_g, Ω_t, t_t y t_{em} is the moment of inertia of the wind turbine, moment of inertia of the electric generator, angular velocity of the turbine, mechanical torque and electromagnetic torque, respectively.

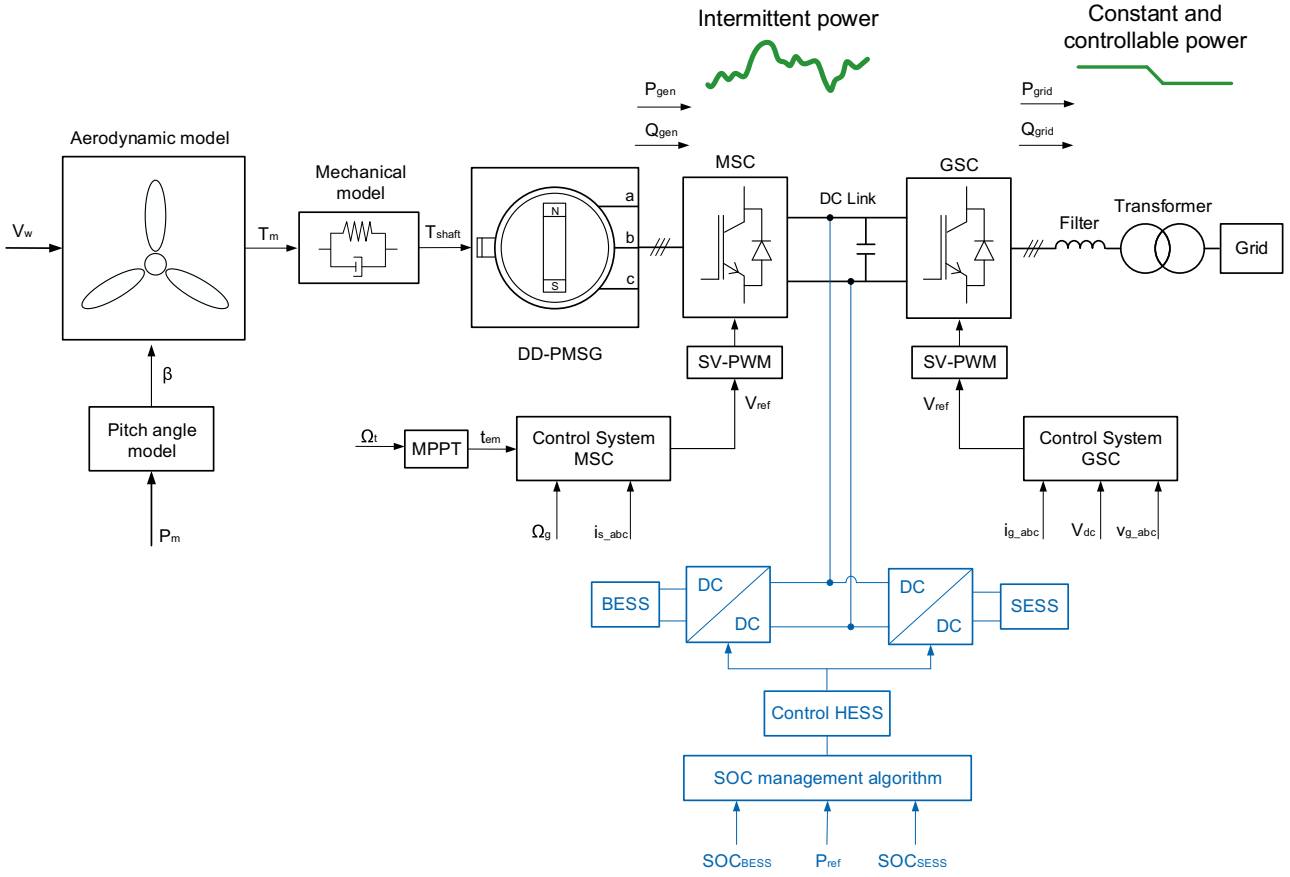

Fig. 2. Schematic of the wind energy conversion system integrated with a hybrid energy storage system.

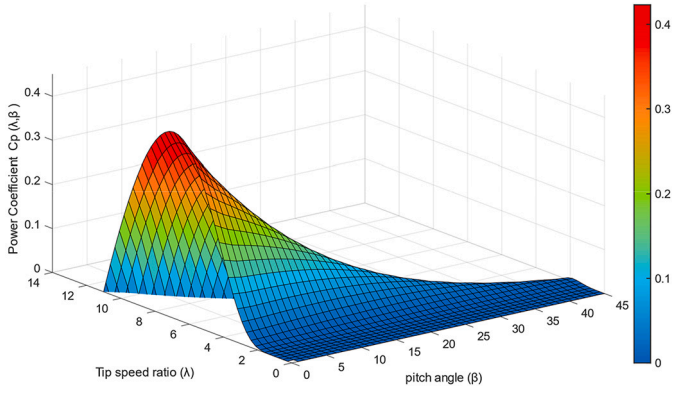

Fig. 3. Power coefficient surface.

3.3. PMSG generator model

The PMSG generator model can be written in a reference frame dq0. This reference frame is orthogonal and rotating with angular displacement θ_s. A balanced three-phase system is assumed, so the zero-sequence component cancels. The generator parameters are shown in Table A.2 in Appendix A. The generator voltage equations are as follows [18]:

$$v_{sd} = r_s i_{sd} + L_d \frac{di_{sd}}{dt} - L_q \omega_r i_{sq} \tag{9}$$

$$v_{sq} = r_s i_{sq} + L_q \frac{di_{qs}}{dt} + L_d \omega_r i_{sd} + \omega_r \psi_{pm} \tag{10}$$

$$\omega_e = p\omega_m \tag{11}$$

where v_{sd} and v_{sq} are the stator voltages on the dq axis, i_{sd} and i_{sq} are the stator currents on the dq axis, L_d and L_q are the inductances on the dq axis, r_s is the stator resistance, ω_r is the electrical speed, ω_m is the mechanical speed, p is the pole pairs of the generator and ψ_{pm} is the magnetic flux of the permanent magnet. The electromagnetic torque of the PMSG is defined by Eq. (12):

$$t_{em} = \frac{3}{2} p\left[\psi_{pm} i_{sq} + \left(L_d - L_q\right) i_{sd} i_{sq}\right] \tag{12}$$

3.4. Machine side converter control (MSC)

The vector control of the permanent magnet synchronous generator is developed in the synchronous rotating frame dq. The principal aim of the MSC is to adjust the wind turbine speed to its optimum value for maximum energy extraction [19,20]. Fig. 4 shows the schematic of the machine-side converter control.

Since the d-axis current component reference (i_{sd_ref}) is set to zero, a proportional relationship between the q-axis current component reference (i_{sq_ref}) and the electromagnetic torque reference (t_{em_ref}) can be obtained.

$$i_{sq\_ref} = (k_t)\left(t_{em\_ref}\right) \;;\; k_t = \frac{2}{3p\psi_{pm}} \tag{13}$$

Eq. (13) shows that the stator current in the q-axis is proportional to the electromagnetic torque produced by the generator.

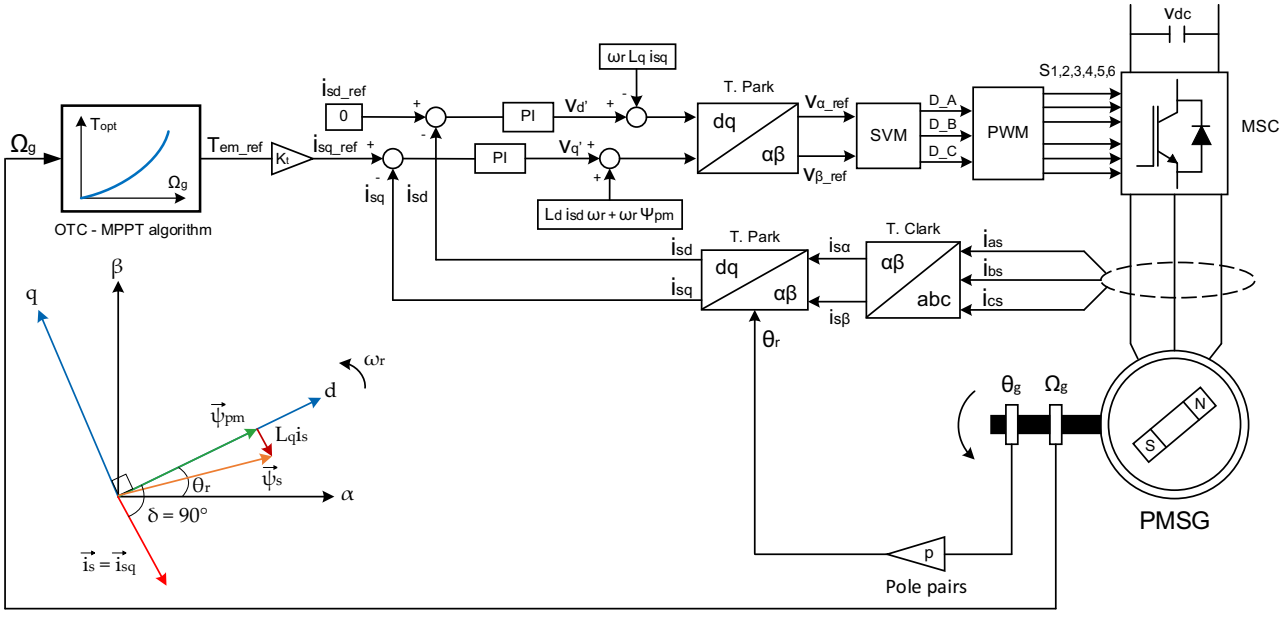

Fig. 4. Machine side converter control scheme (MSC).

3.5. Grid side converter control (GSC)

The main function of the GSC is to keep the link capacitor voltage (v_{cd}) constant between the converters in back-to-back connection, independently of the power control performed by the machine-side converter (MSC). Furthermore, it controls the power factor of the wind turbine [19,20]. Fig. 5 shows the control scheme of the grid-side converter.

To simplify the equations, the d-axis of the dq reference frame is aligned with the grid voltage space vector ($\vec{v}_g$). Because to this condition, the active and reactive power of the grid is proportional to the current components on the dq-axis independently.

$$P_g = \frac{3}{2}\left(v_{dg} i_{dg}\right) = \frac{3}{2}\left(\left|\vec{v}_g\right| i_{dg}\right) \tag{14}$$

$$Q_g = -\frac{3}{2}\left(v_{dg} i_{qg}\right) = -\frac{3}{2}\left(\left|\vec{v}_g\right| i_{qg}\right) \tag{15}$$

Eqs. (14) and (15) show that the active and reactive power are proportional to the stator current in the d-axis (i_{dg}) and q-axis (i_{qg}) respectively.

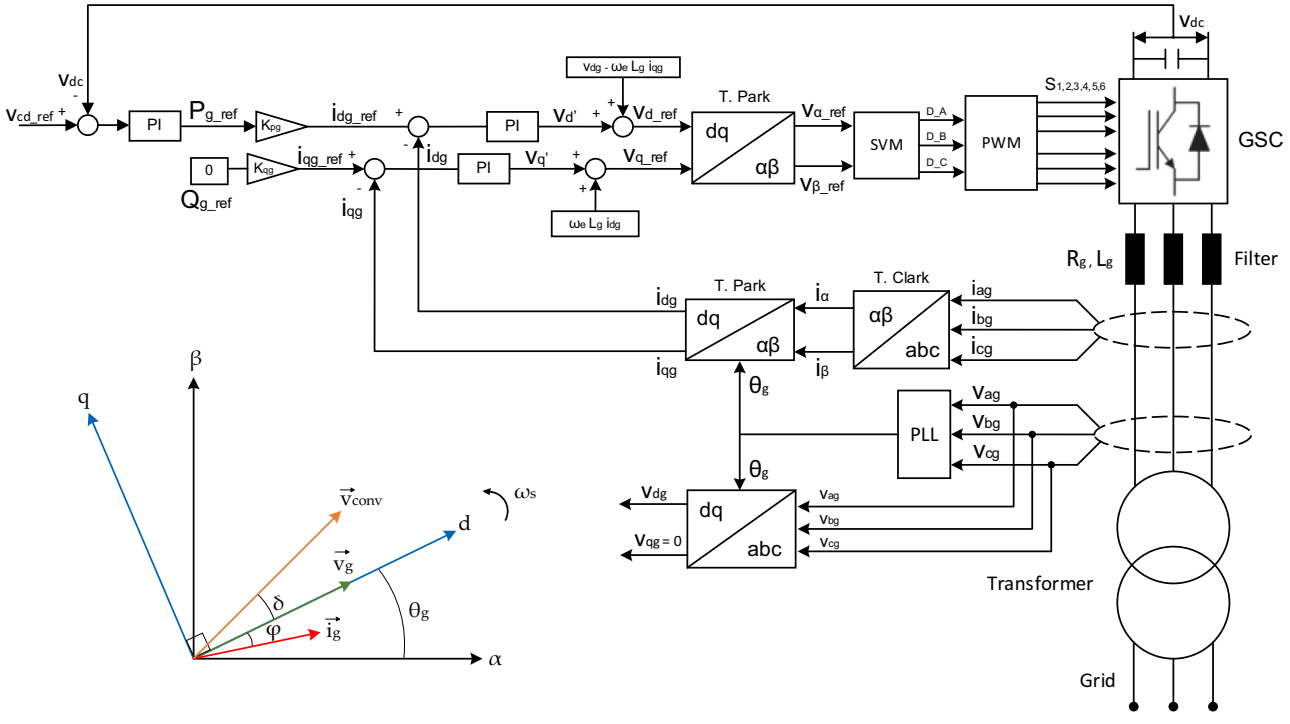

Fig. 5. Grid side converter control scheme (MSC).

3.6. Maximum power point tracking (MPPT)

This optimization method generates a reference electromagnetic torque signal to maximize power extraction under all conditions. Optimal torque control (OTC) regulates the generator torque to its optimum value at different wind speeds to follow the maximum power point. However, the maximum value of the power coefficient and the optimum value of the tip speed ratio need to be known. The Fig. 6 shows the schematic of the OTC [21,22].

The expression that relates the optimum power as a function of the angular speed of the generator is:

$$t_{em\_ref} = \frac{1}{2}\rho\pi R^5 \frac{C_{p\_max}}{\lambda_{opt}^3}\Omega_g^2 = k_{opt}\Omega_g^2 \quad (16)$$

where C_{p_max} is the maximum power coefficient, λ_{opt} is the optimal tip speed ratio, k_{opt} is the optimization constant and Ω_g is the angular velocity of the generator. The value of C_{p_max} and λ_{opt} can be calculated by mathematical or graphical methods. Eq. (16) shows that the optimum torque developed on the shaft is proportional to the mechanical angular velocity of the generator raised to the second power.

4. DC/DC converter connected to the wind turbine

Fig. 7 shows the fundamental topology of a bidirectional converter for absorbing or delivering power to the DC bus. This type of converter is chosen due to its robustness and simplicity [23]. The main drawback is the current on the high voltage side (HVS), which is in the discontinuous conduction mode. Therefore, sufficient filtering capability is required to smooth the pulsed current of the converter. The inductor stores and delivering energy according to the operating states of the IGBTs. The inductance L_p is calculated so that it meets the design conditions in Buck mode and in Boost mode. Similarly, the high voltage side filter capacitance (C_{HVS}) and low voltage side filter capacitance (C_{LVS}) meet the ripple current, ripple voltage and continuous mode conduction conditions. The operating voltage of the BESS varies around 680 V, while the operating voltage of the SESS is variable and reaches a maximum value of 700 V and a minimum value of 100 V. The design parameters of the DC/DC converter are shown in Tables A.3 and A.4 in Appendix A.

5. Control of the hybrid energy storage system

The energy storage system connected to the DC bus controls the intermittent power that the wind turbine injects into the grid. To achieve this, the BESS aims to store and deliver a large amount of energy slowly, leaving the fast dynamics of energy absorption and delivery to the SESS [24]. Eq. (17) establishes the reference signal for the HESS.

$$P_{ref\_HESS} = P_{ref\_grid} - P_{gen} \quad (17)$$

where P_{ref_grid} is the constant and controllable reference power signal delivered to the grid and P_{gen} is the power generated by the wind turbine delivered by the machine side converter. If P_{ref_HESS} is positive, the HESS delivers power to the DC bus and if it is negative; the HESS absorbs power from the DC bus. In this way, constant power is maintained across the DC bus around the set constant reference power. Fig. 8 shows the control scheme to get the reference signals P_{ref_BESS} and P_{ref_SESS}.

Through several tests performed with different time constants for the

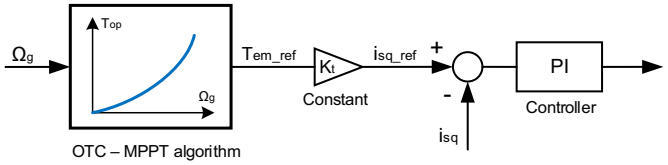

Fig. 6. Schematic of optimal torque control (OTC).

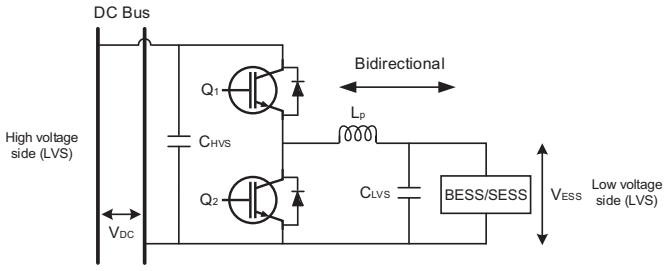

Fig. 7. Bidirectional DC/DC converter.

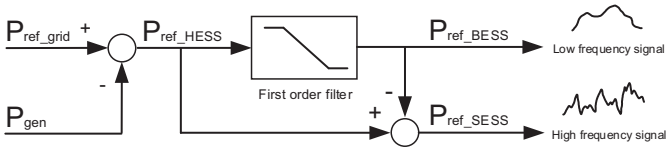

Fig. 8. Scheme to obtain the control signals of BESS and SESS.

first-order filter (τ), a value equal to 140 s was obtained. With this value, an operating balance between the batteries and the supercapacitors is got. Thus, the supercapacitors damp the high-frequency power fluctuations, leaving most of the energy storage or delivery to the batteries [25]. In conclusion, if the time constant is >140 s, the HESS focuses its operation on the SESS and if it is less on the BESS. Fig. 9 shows the internal current loop for the BESS and the SESS. The reference power signals are divided by their respective voltages to get the reference current for the batteries and supercapacitors. These reference current signals are compared with the actual currents and the errors are sent to their respective PI controllers [26].

6. State-of-charge management algorithm of HESS

The state-of-charge management of the hybrid energy storage system is a key factor in ensuring the controllability and stability of the active power delivered by the wind turbine. The control logic depends on the state-of-charge dynamics of the BESS (SOC_{BESS}) and SESS (SOC_{SESS}). The aim is to prevent the BESS and the SESS from being fully charged or discharged by supporting each other in critical situations. Next, the control algorithm for the state-of-charge of the HESS is proposed and developed.

6.1. State-of-charge management algorithm of BESS

Its primary purpose is to automatically control the reference power signal P_{ref_grid} based on the SOC_{BESS}. In this way, the batteries maintain a good state of charge, avoiding deep charge/discharge cycles, which prolongs their useful life. To develop the control algorithm, Eq. (18) defines the parameter σ_p:

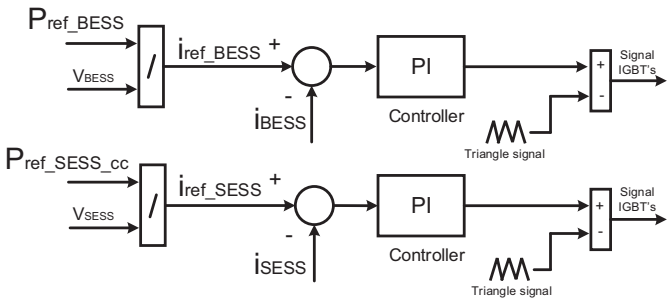

Fig. 9. Scheme to get the control signals of BESS and SESS.

$$\sigma_p = \left| P_{ref\_grid\_ini} - P_{gen} \right| \quad (18)$$

where σ_p is the power threshold, $P_{ref\_grid\_ini}$ is the initial value of the constant and controllable reference power signal delivered to the grid set by the wind power plant operator. Also, σ_{p_ref} is defined as the reference power threshold that serves as the basis for the control algorithm. Three operating zones are determined based on SOC_{BESS}.

6.1.1. Zone 1B ($SOC_{BESS} \leq 20\%$)

To avoid fully discharging the BESS, the signal P_{ref_grid} decreases until P_{gen} is greater than or equal to P_{ref_grid}. This condition causes the BESS to charge, increasing the SOC_{BESS} little by little until it automatically returns to zone 2B. Fig. 10 illustrates the concept of operation of the BESS in zone 1B.

When the SOC_{BESS} reaches 20 %, and the condition that BESS continues to deliver energy is fulfilled, the signal P_{ref_grid} decreases by a straight line until the SOC_{BESS} stops decreasing, i.e., until P_{gen} is greater than or equal to P_{ref_grid}. The algorithm will constantly search for such a solution until the SOC_{BESS} exceeds 20 % and returns to the zone 2B. As long as P_{gen} is greater than P_{ref_grid}, the BESS absorbs energy, which causes the SOC_{BESS} to increase. The slope value (m_{1B}) is variable and depends on the SOC_{BESS}. Fig. 11 shows how the slope increase as the SOC_{BESS} decreases, thus ensuring that the algorithm finds the solution before the SOC_{BESS} reaches 5 %. When P_{ref_grid} is close to P_{gen} (<0.1 MW), the algorithm automatically switches to a smoother slope (50 kW/min) to avoid abrupt changes due to a large slope.

6.1.2. Zone 2B ($20\% < SOC_{BESS} < 90\%$)

If the value of σ_p is less than σ_{p_ref}, then $P_{ref\_grid\_ini}$ does not undergo any change. Conversely, if σ_p is greater than σ_{p_ref}, the value of $P_{ref\_grid\_ini}$ changes slowly until σ_p returns to a value less than σ_{p_ref}. Fig. 12 illustrates the concept of BESS operation in zone 2B.

For this zone, the setting depends on whether P_{ref_grid} is greater or less than P_{gen} to keep σ_p within the proper range. If, P_{ref_grid} is greater than P_{gen}, the slope of the line is negative and if P_{ref_grid} is less than P_{gen}, the slope is positive. The delay time is to avoid unnecessary changes of P_{ref_grid} caused by wind gusts. If after the delay time has elapsed (30 s), the value of σ_p is still higher than σ_{p_ref}, then from then on, the signal P_{ref_grid} change is performed. The value of the slope (m_{2B}) must be chosen in such a way that it does not cause frequency variations in the system with a slower rate of change than zones 1B and 3B. The value chosen is 50 kW/min.

6.1.3. Zone 3B ($SOC_{BESS} \geq 90\%$)

To avoid fully charging the BESS, the signal P_{ref_grid} increases until P_{gen} is less than or equal to P_{ref_grid}. This condition causes the BESS to charge, decreasing the SOC_{BESS} little by little until it automatically returns to zone 2B. Fig. 13 illustrates the concept of operation of the BESS in zone 3B.

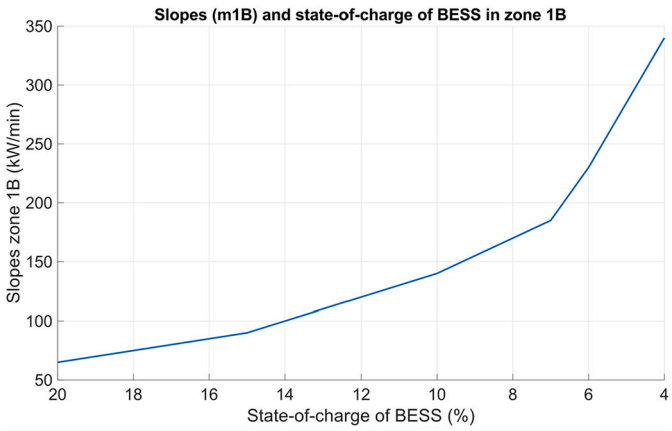

Fig. 11. Slopes (m_{1B}) and state-of-charge of BESS in zone 1B.

When the SOC_{BESS} reaches 90 % and the condition that BESS continues to absorb energy is fulfilled, the signal P_{ref_grid} increases by a straight line until the SOC_{BESS} stops increasing, i.e., until P_{gen} is less than or equal to P_{ref_grid}. The algorithm will constantly search for such a solution until the SOC_{BESS} is <90 % and automatically returns to zone 2B. As long as P_{gen} is less than P_{ref_grid}, the BESS delivers energy, which causes the SOC_{BESS} to decrease. The slope value (m_{3B}) is variable and depends on the SOC_{BESS}. Fig. 14 shows how the slope increase as the SOC_{BESS} increases, thus ensuring that the algorithm finds the solution before the SOC_{BESS} reaches 100 %. When P_{ref_grid} is close to P_{gen} (<0.1 MW), the algorithm automatically switches to a smoother slope (50 kW/min) to avoid abrupt changes due to a large slope.

Fig. 15 shows the flow chart of the BESS state-of-charge management algorithm.

6.2. State of charge management algorithm of SESS

The aim of the algorithm for SESS state-of-charge management is to avoid total SESS charging/discharging and to ensure generation stability. The SOC_{SESS} depends on its voltage (nominal voltage of the SESS equal to 700 V), therefore a very low SOC_{SESS} near 10 % shows that the voltage reaches a value around 70 V. This means a current of very large magnitude for a required power, so the algorithm prevents the SOC_{SESS} from reaching small values. If the SOC_{SESS} is <20 %, the algorithm keeps the SOC_{SESS} stable between 20 % and 10 %, which prevents the voltage from taking values lower than 70 V. On the other hand, if the SOC_{SESS} is >95 %, the algorithm prevents the SOC_{SESS} from reaching 100 %. A

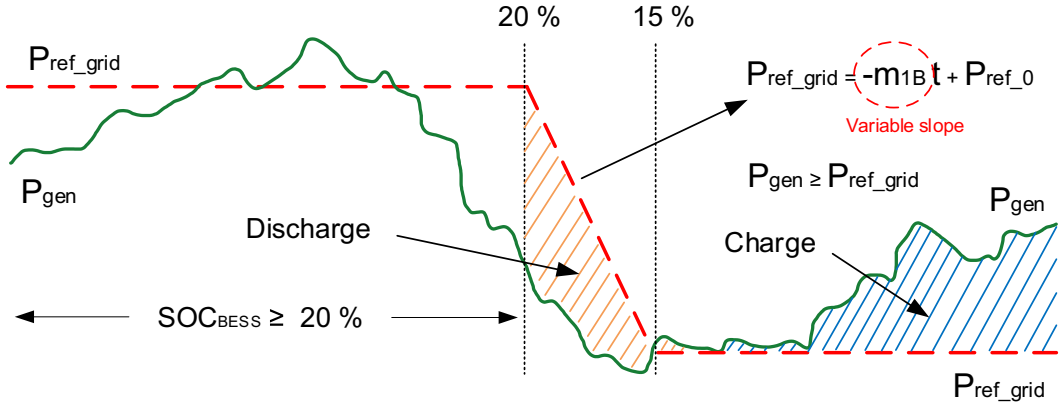

Fig. 10. Operating concept zone 1B.

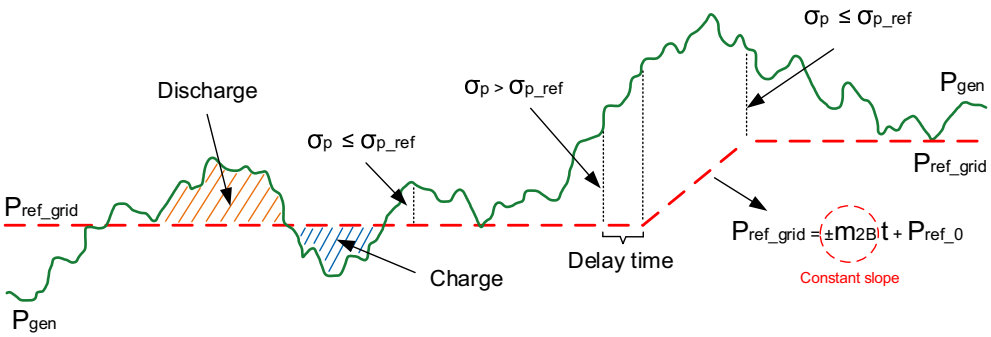

Fig. 12. Operating concept zone 2B.

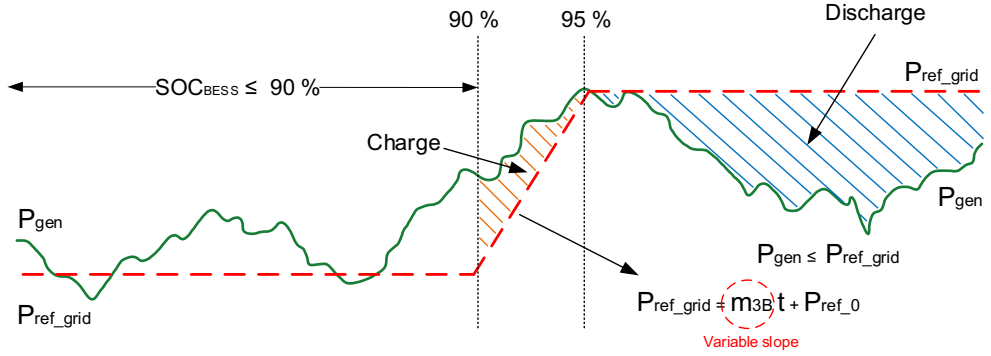

Fig. 13. Operating concept zone 3B.

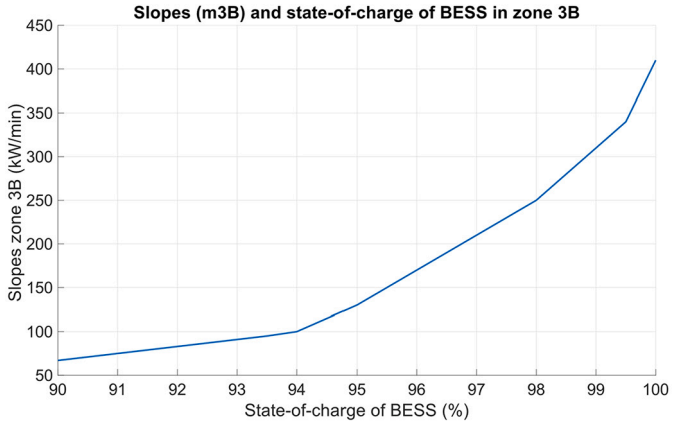

Fig. 14. Slopes (m_{3B}) and state-of-charge of BESS in zone 3B.

control based on the continuous change of the reference power curves of both the BESS and the SESS slowly is proposed to avoid power peaks or transients in the BESS and in the power injected to the power grid. Fig. 16 shows the control scheme that serves as the basis for managing the SOC_{SESS}.

The following equation can be derived from Fig. 16:

$$P_{ref\_BESS}{}' = P_{ref\_BESS} + \left(P_{ref\_SESS\_uc} - P_{ref\_SESS\_cc}\right) \tag{19}$$

where $P_{ref\_BESS}{}'$ is the net reference signal of the BESS, $P_{ref\_SESS\_uc}$ is the uncontrolled SESS reference signal from the filter and $P_{ref\_SESS\_cc}$ is the controllable SESS reference power signal of the SESS state-of-charge management algorithm. While the SESS is in normal operation, the power signal $P_{ref\_SESS\_uc}$ is equal to $P_{ref\_SESS\_cc}$. Three operating zones are defined depending on the SOC_{SESS}.

6.2.1. Zone 1S ($SOC_{SESS} \leq 20\%$)

To avoid total discharge of the SESS, the BESS supports the SESS only in discharge mode by continuously changing the reference signal. The signal $P_{ref\_SESS\_cc}$ decreases and is added to the $P_{ref\_BESS}{}'$ signal progressively by a negatively sloped straight line. Fig. 17 shows the concepts of operation of zone 1S. At point A, the SOC_{SESS} reached 20 %; from that point, the algorithm decreases the signal $P_{ref\_SESS\_cc}$ until it reaches point B. During the change, $P_{ref\_BESS}{}'$ is increasing until $P_{ref\_SESS\_cc}$ is zero. Then the signal $P_{ref\_BESS}{}'$ is equal to the sum of signals P_{ref_BESS} and $P_{ref\_SESS\_uc}$. This condition is only satisfied until the signal $P_{ref\_SESS\_uc}$ changes direction and, from that moment on, the signals $P_{ref\_SESS\_uc}$ and $P_{ref\_SESS\_cc}$ become equal. This occurs at point C, where the SESS absorbs energy to gradually increase the SOC_{SESS} until 20 % and returns to the zone 2S automatically.

- Slope calculation m_{1s}

The slope calculation is based on the available SESS energy between 20 % and 10 % of the SOC_{SESS}. Approximately, the voltage around 20 % is equal to 140 V and at 10 % is equal to 70 V. Then, the available energy of the SESS between 20 % and 10 % is defined by Eq. (20).

$$\Delta E_{20\%-10\%} = \frac{1}{2} C_{SESS}\left(v_{20\%}^2 - v_{10\%}^2\right)$$
$$\Delta E_{20\%-10\%} = \frac{1}{2}(1050)\left(140^2 - 70^2\right) = 7.71\ \text{MJ} \rightarrow 2.14\ \text{kWh} \tag{20}$$

Fig. 18 shows the energy that the SESS has to discharge before the signal $P_{ref\_SESS\_cc}$ is equal to zero.

To prevent the SOC_{SESS} from discharging <10 %, a condition is set that the energy between 20 % and 10 % of the SESS must be greater than or equal to the yellow-colored area.

$$\Delta E_{20\%-10\%} \geq E_d \tag{21}$$

where E_d is the energy that the SESS manages to discharge before

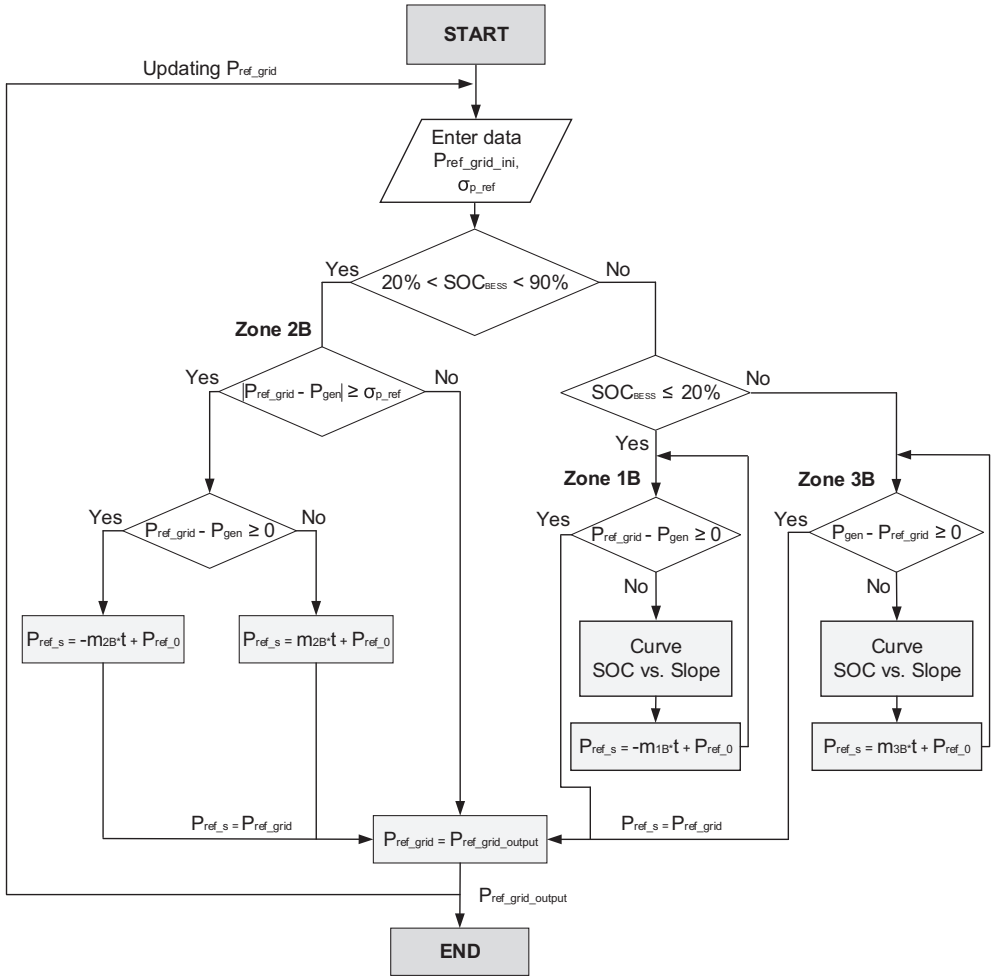

Fig. 15. Flowchart of the BESS state-of-charge management algorithm.

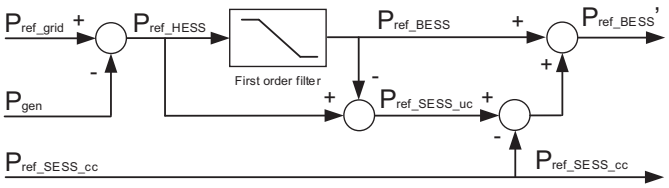

Fig. 16. Reference power signals for SESS state-of-charge management.

$P_{ref\_sess\_cc}$ is zero. Then, the calculation of E_d can be approximated to the area of a triangle.

$$E_d = \frac{1}{2}(P_{SESS\_0})(t_{ds}); \quad t_{ds} = \frac{P_{SESS\_0}}{m_{1s}} \tag{22}$$

where P_{SESS_0} is the SESS power when it reaches 20 % and t_{ds} is the SESS discharge time. To ensure that SOC_{SESS} does not decrease <10 %, the algorithm chooses the most appropriate slope (m_{1s}) that depends on the value of the SESS power just before reaching the lower limit of the SOC_{SESS}. Therefore, it is divided into 7 operating zones with 7 slopes. The change between $P_{ref\_SESS\_cc}$ and $P_{ref\_SESS\_uc}$ signals is executed around 1 min to avoid transients or power peaks affecting the BESS. Table 2 shows the summary of the 7 slopes programmed for zone 1S.

6.2.2. Zone 2S (20 % < SOC_{SESS} < 95 %)

This is the normal operating zone. There is no restriction on the SESS reference power signal. It is satisfied that the signal $P_{ref\_SESS\_cc}$ is equal to $P_{ref\_SESS\_uc}$.

$$P_{ref\_SESS\_cc} = P_{ref\_SESS\_uc} \tag{23}$$

6.2.3. Zone 3S ($SOC_{SESS} \geq$ 95 %)

To avoid full charging of the SESS, the BESS supports the SESS only in charging mode by continuously changing the reference signal. The signal $P_{ref\_SESS\_cc}$ increases and is added to the signal P_{ref_BESS}' progressively by a positively sloping straight. Fig. 19 shows the concept of operation of the zone 3S. At point A, the SOC_{SESS} reaches 95 %; thereafter, the algorithm increases the signal $P_{ref\_SESS\_cc}$ until point B is reached. When $P_{ref\_SESS\_cc}$ reaches point B, the signal P_{ref_BESS}' is the sum of the signals $P_{ref\_SESS\_uc}$ and P_{ref_BESS}. This condition is only fulfilled until the signal $P_{ref\_SESS\_uc}$ changes direction and thereafter the signals $P_{ref\_SESS\_uc}$ and $P_{ref\_SESS\_cc}$ are equal. This occurs at point C, where the SESS begins to supply energy gradually decreasing the SOC_{SESS} to 95 % and returns to the zone 2S automatically. The zone 3S has a smaller operating range than the 1S zone because it has more available energy.

- Slope calculation m_{3s}

The slope calculation is based on the available SESS energy has between 95 % and 100 % of the SOC_{SESS}. Approximately, the voltage around 95 % is equal to 665 V and at 100 % is equal to 700 V. Then, the available SESS energy between 95 % and 100 % is defined by Eq. (24).

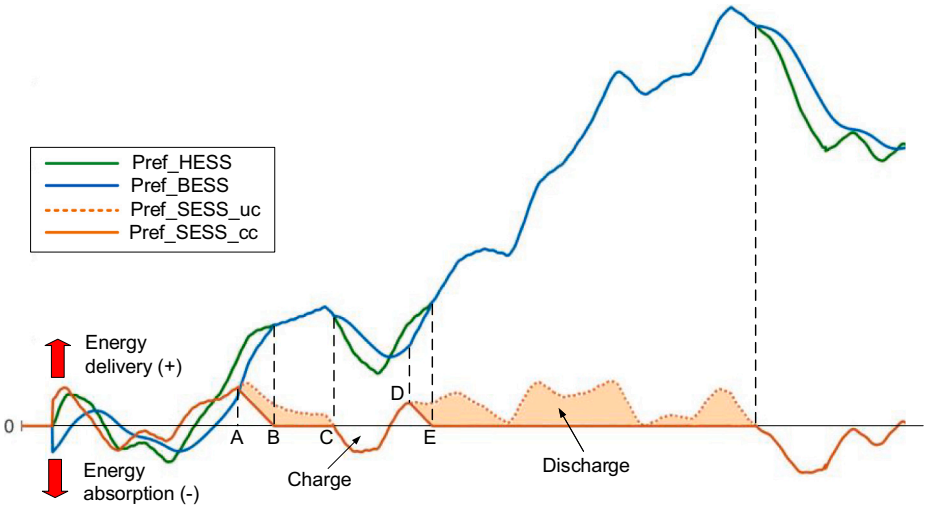

Fig. 17. Operating concept zone 1S.

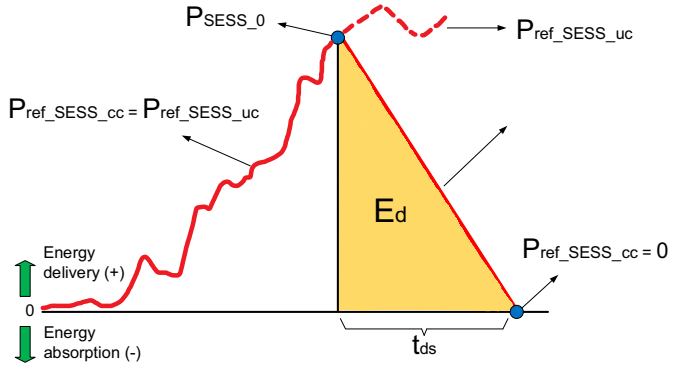

Fig. 18. SESS discharge energy (E_d).

Table 2
Summary of slope calculation zone 1S.

Zones [kW]	$m_{1s}\left[\frac{kW}{min}\right]$	t_{max} [s]	SOC_{min} [%]	Minimum voltage [V]
$300 \leq P_{SESS\_0}$	570.00	40.0	10.22	71.58
250–300	360.00	50.0	10.41	72.90
200–250	250.00	60.0	10.41	72.90
150–200	200.00	60.0	12.91	90.40
100–150	150.00	60.0	15.00	105.02
50–100	100.00	60.0	16.83	117.84
$P_{SESS\_0} < 50$	50.00	60.0	18.48	129.39

$$\Delta E_{95\%-100\%} = \frac{1}{2} C_{SESS}\left(V_{95\%}^2 - V_{100\%}^2\right)$$
$$\Delta E_{95\%-100\%} = \frac{1}{2}(1050)\left(665^2 - 700^2\right) = 25.08\ \text{MJ} \rightarrow 6.96\ \text{kWh} \quad (24)$$

Fig. 20 shows the energy charged by the SESS before the signal $P_{ref\_SESS\_cc}$ is equal to zero.

To prevent the SOC_{SESS} from charging to 100 %, a condition is set that the energy between 95 % and 100 % of the SESS must be greater than or equal to the yellow color zone.

$$\Delta E_{95\%-100\%} \geq E_c \quad (25)$$

where E_c is the energy that the SESS manages to charge before $P_{ref\_SESS\_cc}$ is zero. Then, the calculation of E_c can be approximated to the area of a triangle.

$$E_c = \frac{1}{2}\left(\left|P_{SESS\_0}\right|\right)(t_{cs});\ \ t_{cs} = \frac{\left|P_{SESS\_0}\right|}{m_{3s}} \quad (26)$$

where P_{SESS_0} is the SESS power when it reaches 20 % and t_{cs} is the SESS charge time. To ensure that the SOC_{SESS} does not reach 100 %, the algorithm chooses the most appropriate slope (m_{3s}) which depends on the value of the SESS power just before reaching the lower limit of the SOC_{SESS}. Therefore, it is divided into 7 zones obtaining 7 slopes. The change between $P_{ref\_SESS\_cc}$ and $P_{ref\_SESS\_uc}$ signals is executed around 1 min to avoid transients or power peaks affecting the BESS. Table 3 shows the summary of the 7 slopes programmed for zone 3S.

Fig. 21 shows the flowchart of the SESS state-of-charge management algorithm.

7. HESS sizing

The system is sized for the most unfavorable operating conditions to ensure proper operation. In the hybrid system, the batteries store most of the energy being the base of the system while the supercapacitors store the energy of the power peaks caused by wind gusts and the variability of wind speed. To calculate the energy of the BESS, the power threshold and the operating time of the BESS, which has been set to 1 h, are used. Therefore, the energy storage in the batteries is expressed by Eq. (27).

$$E_{BESS} = \left(\sigma_{p\_ref}\right)\left(t_{op\_BESS}\right)$$
$$E_{BESS} = (0.5\ \text{MW})(1\ \text{h}) = 500\ \text{kWh} \quad (27)$$

The effective capacity of the BESS is the capacity used between a 20 % to 90 % state-of-charge due to the algorithm control. The average voltage of the BESS is equal to 680 V. Therefore, the effective capacity is given by Eq. (28)

$$Q_{BESS\_eff} = \frac{E_{BESS\_eff}}{v_{BESS}} = \frac{500\ \text{kWh}}{680\ \text{V}} = 735.29\ \text{Ah} \quad (28)$$

Approximately, the effective capacity and effective energy represents 78 % of the total capacity and total energy of the BESS.

$$Q_{BESS\_total} = \frac{100\%}{78\%} Q_{BESS\_eff} = 942.67\ \text{Ah} \approx 950\ \text{Ah}$$
$$E_{BESS\_total} = \frac{100\%}{78\%} E_{BESS\_eff} = 641.02\ \text{kWh} \quad (29)$$

The energy stored in the SESS will be 11 % of the total energy of the BESS.

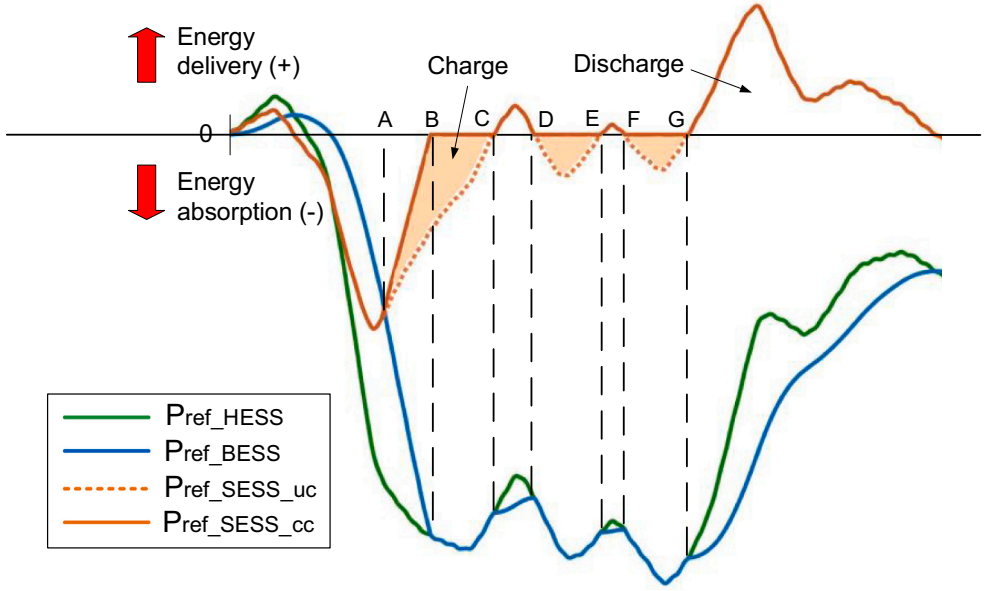

Fig. 19. Operating concept zone 3S.

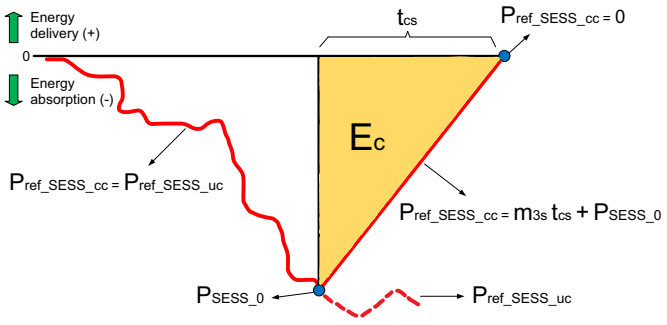

Fig. 20. SESS charge energy (E_c).

Table 3
Summary of slope calculation zone 3S.

Zones [kW]	$m_{3s}\left[\frac{kW}{min}\right]$	t_{max} [s]	SOC_{max} [%]	Maximum voltage [V]
$300 \leq \lvert P_{SESS\_0}\rvert$	380.34	55.2	96.96	679
250–300	300.00	60.0	96.82	678
200–250	250.00	60.0	96.52	676
150–200	200.00	60.0	95.22	674
100–150	150.00	60.0	95.92	671
50–100	100.00	60.0	95.61	669
$\lvert P_{SESS\_0}\rvert < 50$	50.00	60.0	95.31	667

$$E_{SESS\_total} = 11\%\ E_{BESS\_total} \qquad (30)$$

$$E_{SESS\_total} = 70.51\ \text{kWh} \rightarrow 253.8\ \text{MJ}$$

The equivalent capacitance of the SESS is calculated by Eq. (31):

$$C_{SESS} = \frac{2E_{SESS\_total}}{v_{SESS\_nom}} \qquad (31)$$

$$C_{SESS} = \frac{2(253.8\ \text{MJ})}{700^2} = 1035.92\ \text{F} \approx 1050\ \text{F}$$

Summarizing, we have a hybrid energy storage system (HESS) composed of a BESS of 950 Ah with an average voltage of 680 V and a SESS of 1050 F with a nominal voltage of 700 V.

8. Definition of inertia constant and rotational speed of wind turbine

The inertia constant of the wind turbine (H_{wt}) is time-varying because the rotational speed (Ω_g) depends on wind speed variations. Traditionally, the wind turbine inertia constant is defined by the following Eq. (32).

$$H_{wt} = \frac{J_{wt}\Omega_g^2}{2S_n} \qquad (32)$$

where J_{wt} is the moment of inertia of the wind turbine and S_n is the apparent rated power of the wind turbine. If the wind turbine operates integrated to the hybrid energy storage system (HESS) to control the active power, an approximation can be made by Eq. (16) of the optimal torque control (OTC), integrating the active power injected towards the power grid (P_{grid}) and the wind turbine rotational speed (Ω_g) by the following expression:

$$P_{grid} \approx P_{opt} = t_{opt}\Omega_g = k_{opt}\Omega_g^2\Omega_g = \ k_{opt}\Omega_g^3 \qquad (33)$$

Then, the rotational speed of the wind turbine can be expressed as a function of P_{grid} and k_{opt}.

$$\Omega_{gv} = \sqrt[3]{\frac{P_{grid}}{k_{opt}}} \qquad (34)$$

Eq. (34) shows that the wind turbine rotational speed observed from the grid side can be constant and controlled as a function of the active power injected into the grid. Thus, Ω_{gv} is denoted as the virtual rotational speed of the wind turbine as seen from the grid. Replacing Eq. (34) in Eq. (32) gives the following expression:

$$H_{wt\_v} = \frac{J_{wt}P_{grid}^{\frac{2}{3}}}{2k_g\ S_n} \ ; \ \ k_g = k_{opt}^{\frac{2}{3}} \qquad (35)$$

where k_g is the rotating constant and H_{wt_v} is the virtual inertia constant of the wind turbine, as seen from the grid side. Eq. (35) shows that the virtual inertia constant depends on the variation of the power injected into the grid, and since this power is constant and controlled, the result is a virtual inertia constant with small variations.

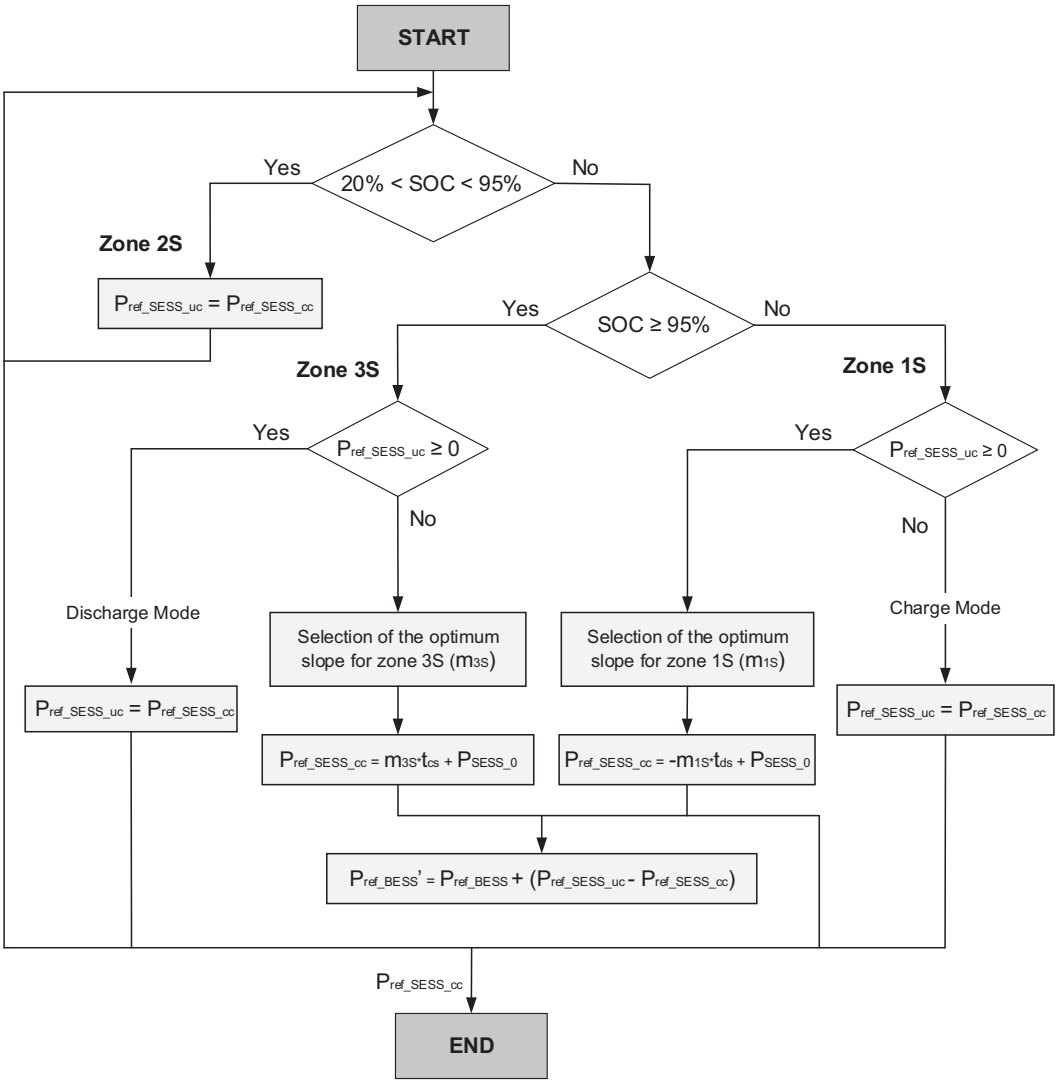

Fig. 21. Flowchart of the SESS state-of-charge management algorithm.

9. Simulation results

For the simulations, a DD-PMSG wind turbine with similar characteristics to the 2.5 MW Goldwind wind turbine, a HESS composed of a BESS (950 Ah) and a SESS (1050 F) and σ_{p_ref} equal to 0.5 MW. The other parameters can be found in Appendix A. Fig. 22 shows the wind speed profiles used for the study simulations.

9.1. Operation with WS1

Fig. 23 shows the active power curves during 6 h of operation. Where P_{grid} is the controlled active power delivered to the grid through the grid side converter (GSC), P_{ref_grid} is the reference signal coming from the SOC management algorithm, P_{gen} is the intermittent active power of the wind turbine, P_{BESS} is the power absorbed or delivered by the BESS and P_{SESS} is the power absorbed or delivered by the SESS. $P_{ref\_grid\_ini}$ is equal to 1.3 MW, the initial SOC_{BESS} is 55 % and SOC_{SESS} is 57 %.

At instant t = 0.26 h, the HESS is connected to the wind turbine through the DC link. From that instant on, the intermittent power delivered by the wind turbine becomes a constant and controlled power due to the HESS absorbs and delivers power to the DC bus. At instant t = 1.81 h, the P_{ref_grid} signal changes from 1.3 MW to 1.13 MW slowly for about 9.6 min and settles to a new operating point automatically. The reason for the change is to avoid deep charge/discharge cycles in BESS. The setting is performed with a delay of 30 s after it detects that σ_p is higher than σ_{p_ref} to avoid unnecessary changes due to wind gusts. Then, from the instant t = 1.97 h, the wind turbine maintains a constant active power. At instant t = 2.53 h, the SOC_{BESS} enters zone 1B, so the charge management algorithm adjusts the power signal P_{ref_grid} to a new operating point equal to 0.77 MW. Moreover, the algorithm prevents the SESS from discharging between instants t = 1.843 h to t = 1.99 h and t = 5.516 h to t = 5.576 h. In addition, further adjustments are observed in the power signal P_{ref_grid} as σ_p again exceeds σ_{p_ref}.

Fig. 24 shows the SOC_{BESS} and SOC_{SESS} profiles. The dynamic of the SOC_{BESS} is slow and does not perform deep discharges, while the dynamics of the SOC_{SESS} is fast. When the SOC_{BESS} is <20 %, the algorithm manages the state-of-charge to prevent the current in the SESS from reaching a high magnitude. On the other hand, when SOC_{BESS} is lower than 20 % and higher than 90 %, the algorithm manages the state-of-charge to prevent the BESS from being fully charged or discharged.

Fig. 25 shows the voltage variation of the BESS and SESS. The BESS voltage variation remains on average around 680 V, with a minimum voltage of 641.7 V and a maximum voltage of 704.3 V. While the SESS voltage has variations between 100 and 680 V due to its higher dependence on its state-of-charge.

Fig. 26 shows the variation of the BESS and SESS current. It is observed that the BESS current are smooth curves, while the SESS current contains the current peaks that are prejudicial to the BESS. When

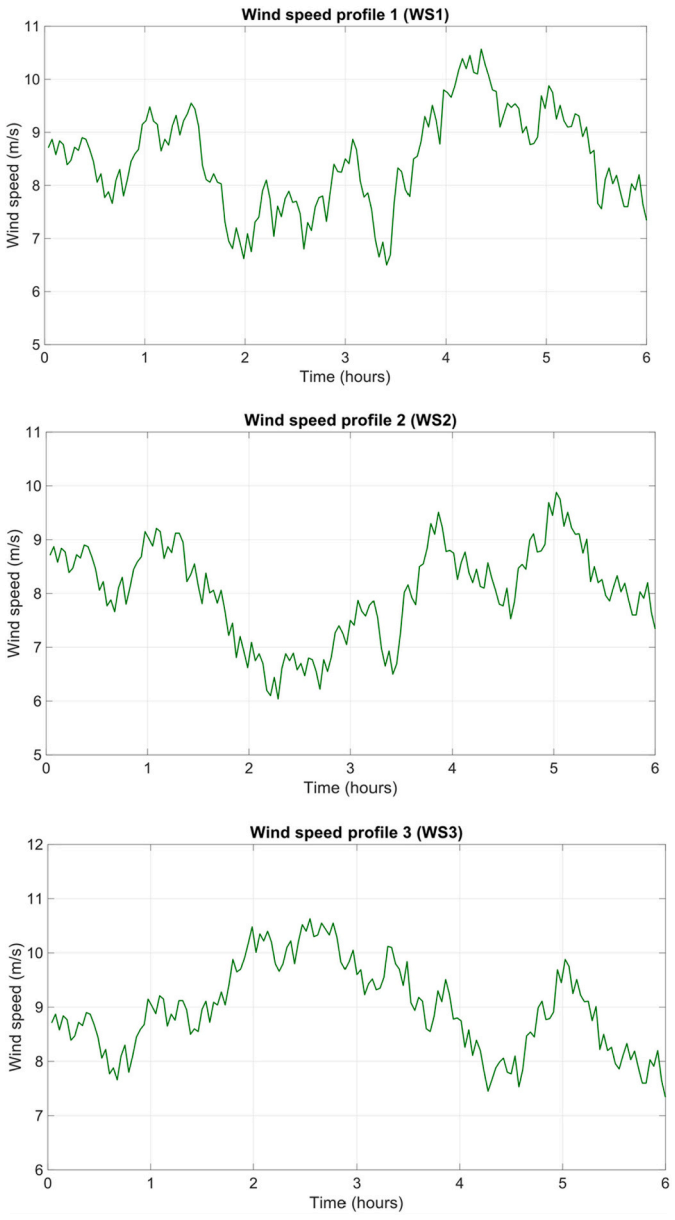

Fig. 22. Wind speed profiles for the simulations, WS1, WS2 and WS3.

the SESS enters the zone 1S, it only works by absorbing the current peaks, while the BESS is responsible for supplying the current peaks. The algorithm ensures that the BESS supports the SESS in critical situations until it automatically returns to zone 2S.

The following are the results of the most important PMSG wind turbine variables with the wind speed profile WS1. Fig. 27 shows the mechanical power (P_m) and power coefficient $C_p(\lambda, \beta)$ of the wind turbine during the 6 h of operation. The optimum torque control (OTC) regulates the electromagnetic torque of the PMSG to its optimum value. The power coefficient remains around 0.438 for different wind speed values.

Fig. 28 shows the variation of the electromagnetic torque and the rotational speed of the wind turbine. The PMSG has 42 pairs of poles and therefore has a maximum rotational speed of 14.5 rpm.

Fig. 29 shows the stator current components on the dq-axis. The reference components i_{ds} is set to zero, while the i_{qs} component is proportional to the electromagnetic torque. This realizes the zero direct-axis current (ZDC) control. While Fig. 30, shows the stator current in the abc reference frame. On the other hand, Fig. 31 shows the voltage on the DC link between the back-to-back converters. The voltage remains constant at around 1300 V with very little variation because the power transmitted across the DC link is controllable.

9.2. *Algorithm operation in critical zones*

In this section, the initial state-of-charge of the BESS is established near zones 1B and 3B to verify how the charge management algorithm maintains the stability of the generation in critical situations. With supercapacitors, as they have a faster charge/discharge dynamics compared to batteries, they can reach the zones 1S and 3S more easily. For this reason, the initial state-of-charge of the SESS can be chosen at any point.

9.2.1. *HESS operation with a SOC < 30 %*

Fig. 32 shows the critical operation of the HESS with an initial SOC_{BESS} equal to 22 % and an initial SOC_{SESS} equal to 28 % with wind speed profile WS2.

At instant t = 0.62 h, the SOC_{BESS} decreases to 20 % entering zone 1B. Therefore, the algorithm decreases the signal P_{ref_grid} from 1.3 MW to 1.05 MW by a negative slope line until P_{gen} is greater than or equal to P_{ref_grid}. At instant t = 2.26 h, the SOC_{BESS} enters zone 1B again, consequently the algorithm again changes the signal P_{ref_grid} to 0.586 MW and remains at this reference until SOC_{BESS} increases and returns to zone 2B. In this way, the BESS is prevented from discharging completely. Other changes in the signal P_{ref_grid} are observed, which follows the same logic but to avoid full battery charging.

Fig. 33 shows the variation of SOC_{BESS} and SOC_{SESS} with the WS2 profile. For the batteries, between instants t = 0.62 h and t = 0.94 h,

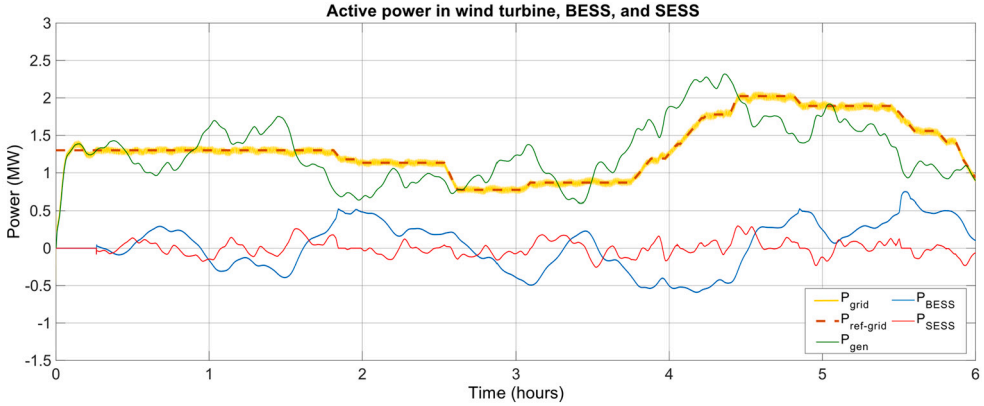

Fig. 23. Power curves with wind speed profile 1 (WS1).

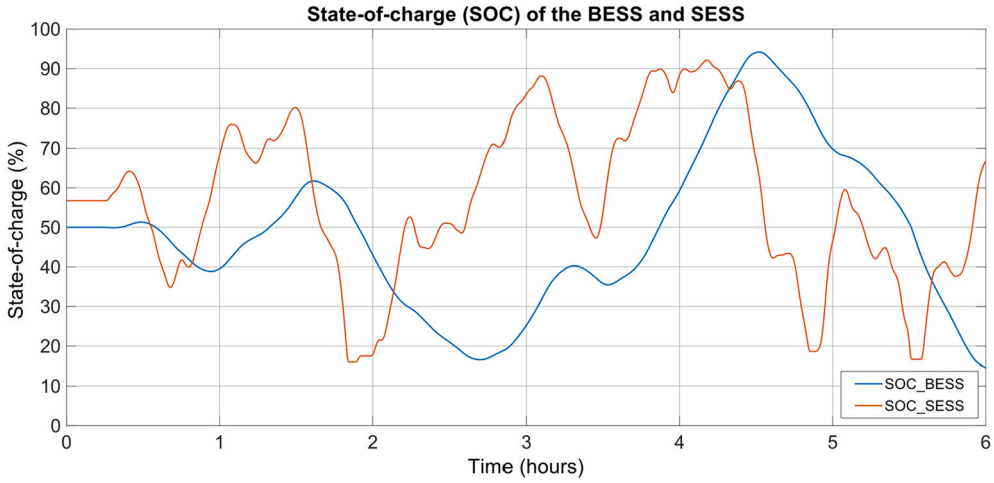

Fig. 24. State of Charge of the BESS and SESS with WS1.

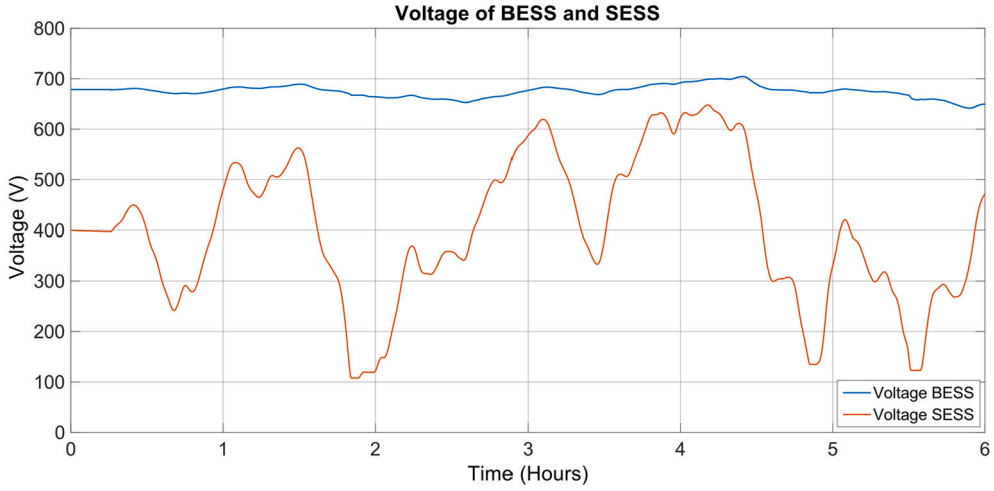

Fig. 25. Voltage BESS and SESS with WS1.

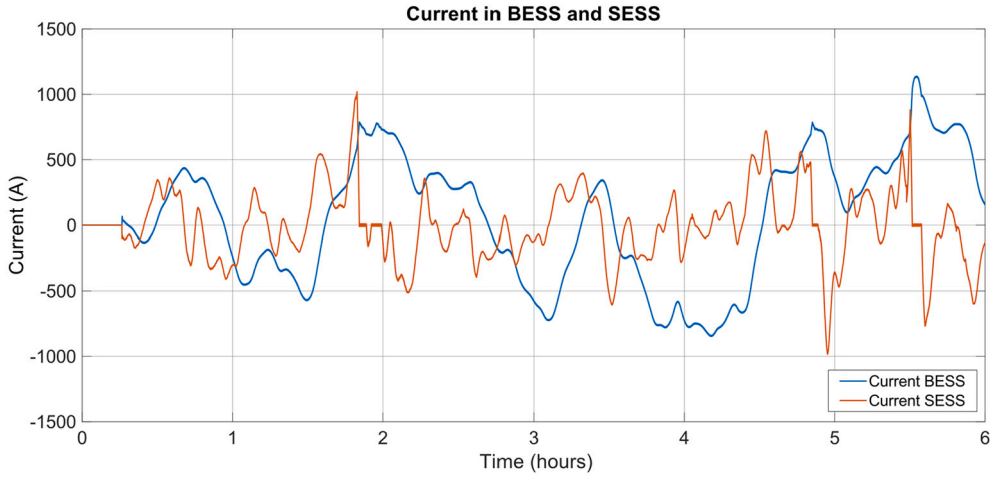

Fig. 26. Current in BESS and SESS with WS1.

SOC_{BESS} enters zone 1B. Similarly, at instant t = 2.26 h, the SOC_{BESS} re-enters zone 1B and at instant t = 3 h, it automatically returns to zone 2B. It then reaches zone 3B at instant t = 5 h, returning to zone 2B at instant t = 5.36 h. For the supercapacitors, the SOC_{SESS} enters zone 1S three times. At instant t = 0.61 h, both SOC_{BESS} and SOC_{SESS} are <20 %, demonstrating that both BESS and SESS can operate in critical situations at the same time.

Fig. 34 shows the power reference signals for HESS, BESS, and SESS.

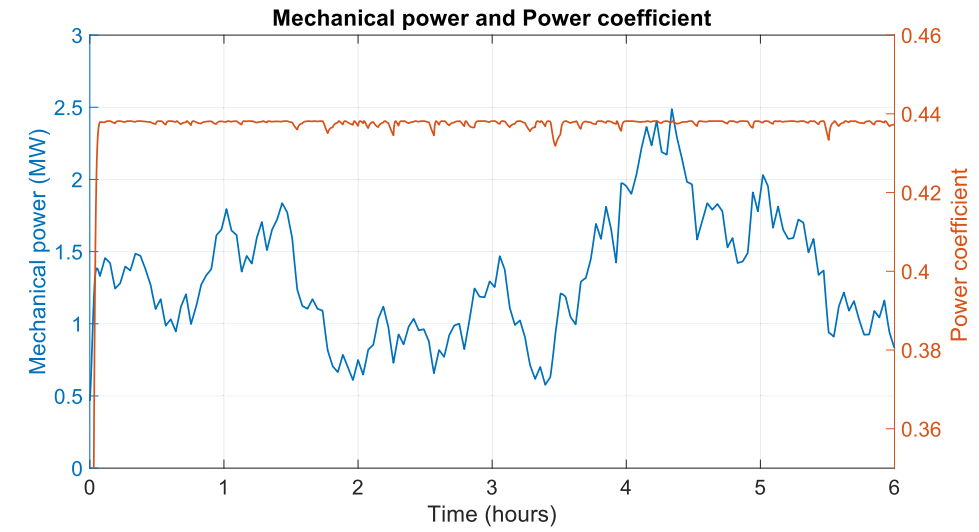

Fig. 27. Mechanical power and Power coefficient with WS1.

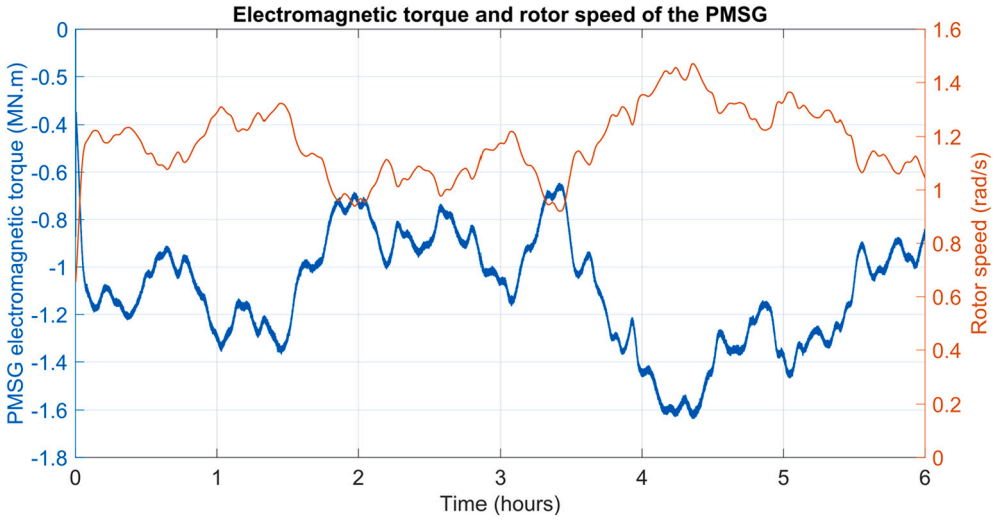

Fig. 28. Electromagnetic torque and rotor speed of the PSMG with WS1.

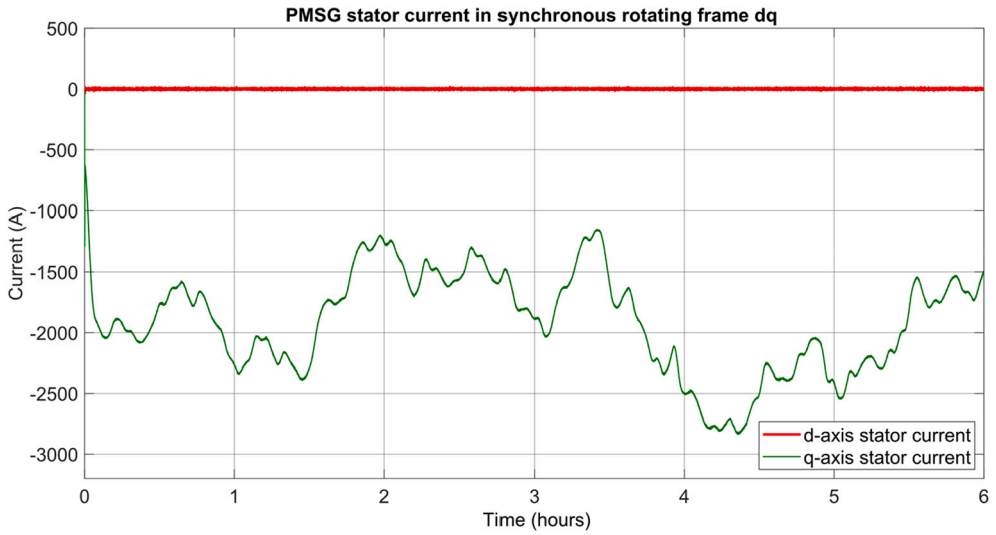

Fig. 29. PMSG stator current in synchronous rotating frame dq with WS1.

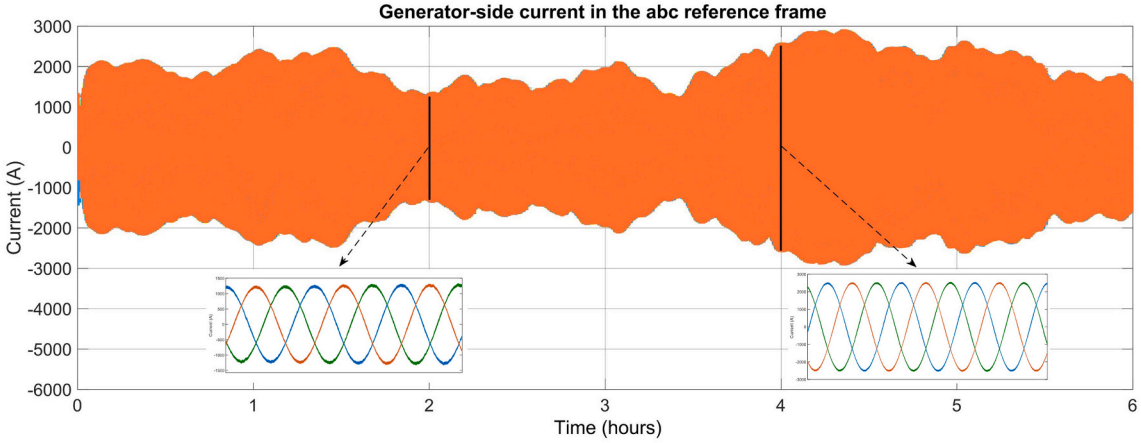

Fig. 30. PMSG stator current in abc reference frame with WS1.

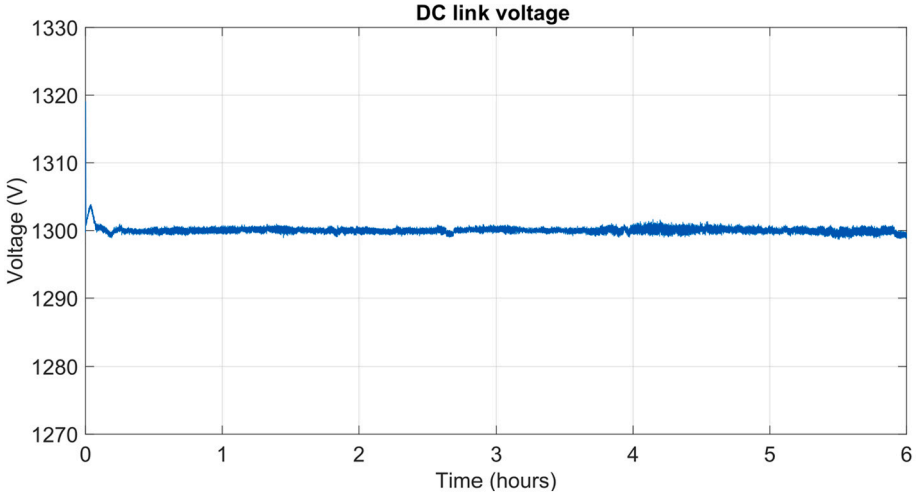

Fig. 31. DC link voltage with WS1.

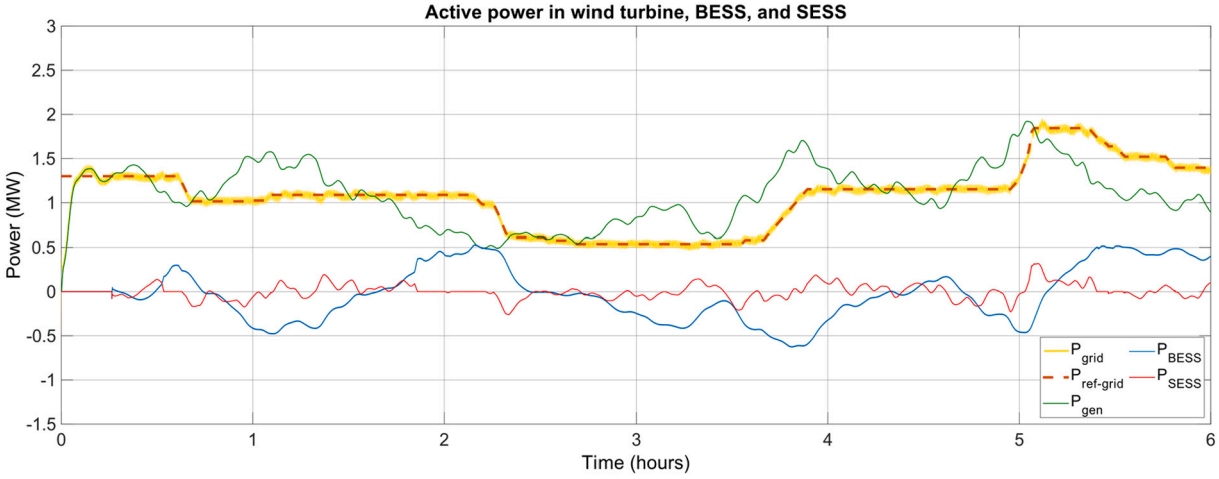

Fig. 32. Power curves with wind speed profile 2 (WS2).

For example, from instant t = 1.86 h to t = 2.21 h, the algorithm controls the signals $P_{ref\_SESS\_cc}$ and P_{ref_BESS} to prevent the SESS from fully discharging. After t = 2.21 h, the $P_{ref\_SESS\_cc}$ signal continues its normal operation, maintaining the stability of the power supplied by the wind turbine.

9.2.2. HESS operation with SOC > 70 %

Fig. 35 shows the critical operation of the HESS with an initial SOC_{BESS} equal to 85 % and an initial SOC_{SESS} equal to 78 % with wind speed profile WS3.

At instant t = 1.72 h, the SOC_{BESS} reaches 90 % entering zone 3B.

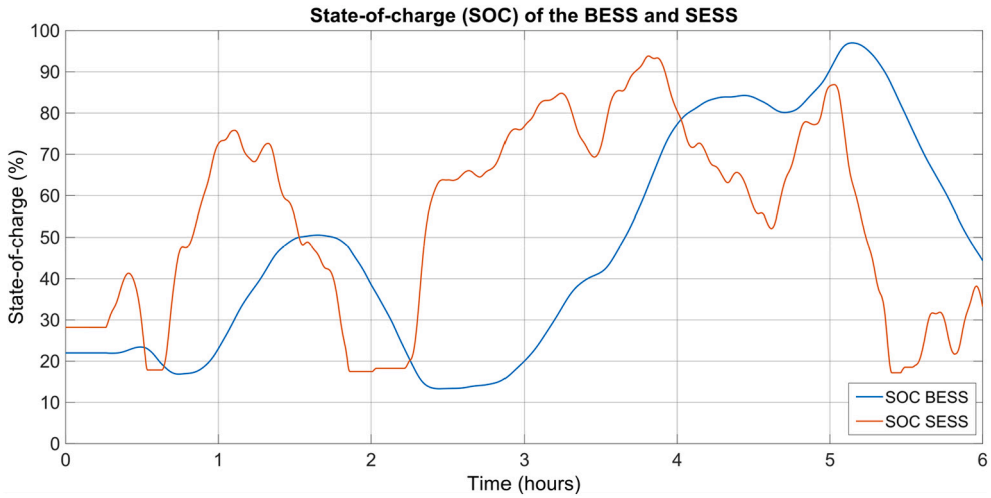

Fig. 33. State of charge of the BESS and SESS with WS2.

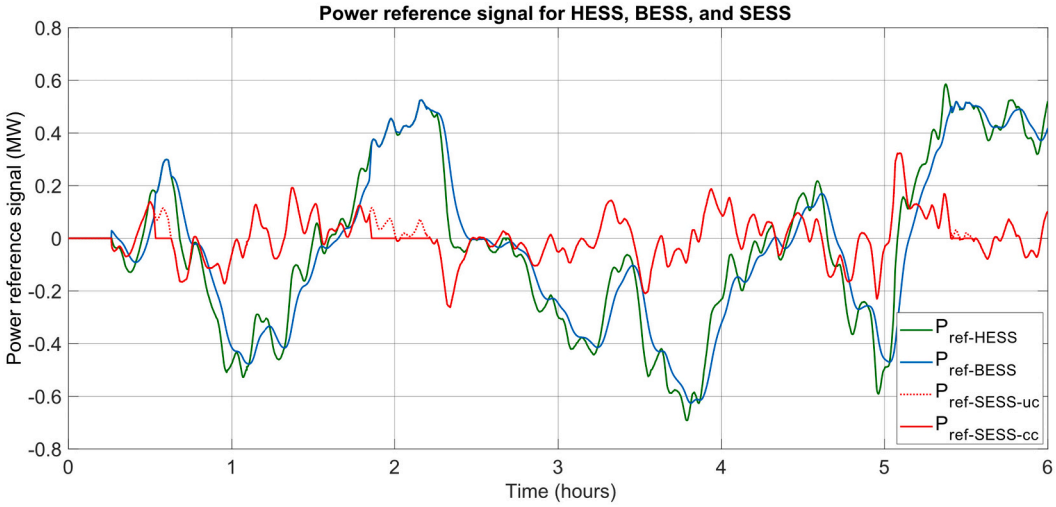

Fig. 34. Reference power signals for HESS, BESS and SESS with WS2.

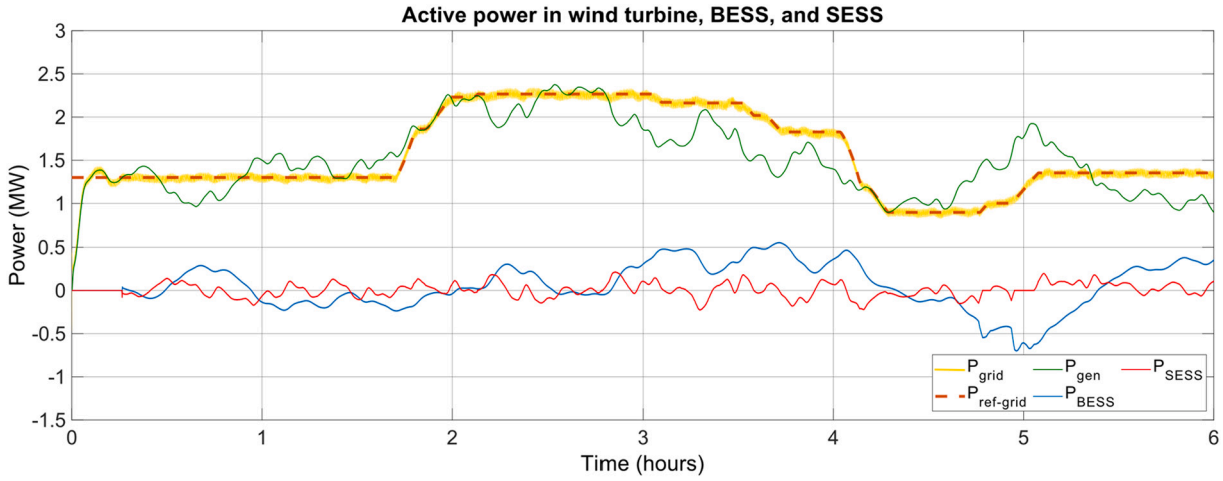

Fig. 35. Power curves with wind speed profile 3 (WS3).

Therefore, the algorithm increases the signal P_{ref_grid} from 1.3 MW to 2.25 MW by a positive slope line until P_{gen} is less than or equal to P_{ref_grid}. At instant t = 4.1 h, the SOC_{BESS} enters zone 1B, consequently, the algorithm decreases the signal P_{ref_grid} to 0.9 MW and remains at this reference until the SOC_{BESS} increases and automatically returns to zone 2B. Other changes observed in the signal P_{ref_grid} is due to σ_p is greater than σ_{p_ref}.

Fig. 36 shows the variation of SOC_{BESS} and SOC_{SESS} with the WS3 profile. For the batteries, between instants t = 1.71 h and t = 2.31 h, the SOC_{BESS} enters zone 3B, where the algorithm prevents the BESS from being fully charged. Then, the SOC_{BESS} automatically returns to zone 2S. Between instants t = 4.05 h and t = 4.79 h, the SOC_{BESS} enters zone 1B and the algorithm prevents the BESS from fully discharging. For the supercapacitors, the SOC_{SESS} enters zone 3S once, where the algorithm prevents its full charge.

Fig. 37 shows the power reference signals for HESS, BESS, and SESS. For example, from instant t = 4.78 h to t = 5.06 h, the algorithm controls the signals $P_{ref\_SESS\_cc}$ and P_{ref_BESS} to prevent the SESS from fully charging. After t = 5.06 h, the signal $P_{ref\_SESS\_cc}$ continues its normal operation, maintaining the stability of the power supplied by the wind turbine.

9.3. Inertia constant and angular velocity of the wind turbine

Fig. 38 shows the variation of the wind turbine angular velocity and wind turbine inertia constant observed from the machine side and from the grid side with the wind speed profile WS1. It is observed that the virtual inertia constant ($H_{wt\_virtual}$) varies slowly as a function of the constant power delivered by the wind turbine.

10. Conclusions and future work

An independent hybrid energy storage system (HESS) integrated into each wind turbine provides greater continuity of operation of a wind power plant. The HESS counteracts the intermittency of wind turbine output power by absorbing or delivering power through the DC link regarding a controllable reference active power. Simulations have shown that the HESS state-of-charge management algorithm complies with ensuring the controllability and stability of the wind-turbine-HESS system at all times. The wind turbines inject a constant and controllable power even in the most critical situations, thanks to the fact that the algorithm searches and slowly adjusts a new operating point automatically. In this work, a HESS composed of electrochemical batteries and supercapacitors has been used as a solution. In a real application, the composition of the HESS can vary depending on several aspects, such as the availability of the technology, the costs, and the dimensions of the installation. Although the results are positive, the main barrier is the cost of the energy storage system. Therefore, its installation can be done gradually to eliminate the intermittency of wind energy during periods of time when the power system requires it. Furthermore, new concepts on the rotational speed and inertia constant of the wind turbine from the grid side have been developed, which will be useful for future electrical studies of wind farm installations with energy storage systems.

After observing the results of the simulations, the following comparisons can be made:

In contrast to the paper [14], in the present paper the BESS and SESS operate simultaneously, with a smooth power curve for the BESS and peak power for the SESS. Furthermore, in critical situations with a state of charge below 20 %, the system can automatically switch to another operating point to continue delivering constant power. The paper, [15], provides a significant concept to control the reference power of the SESS and prevent it from reaching its capacity limits. In the present work, a different concept was used, but with the same aim of avoiding reaching the minimum and maximum limit. For this purpose, the charge and discharge energy of the SESS when it enters the 1S and 3S zones was calculated, evaluating different cases to ensure that the SESS does not reach its minimum or maximum capacity for any reason. In comparison with [16], the present work does not use the concept of a constant power for a time window, since it makes rapid changes in the active power of the wind turbine from one time window to another time window. This could cause variations in the system's frequency. A suitable way is to make power changes slowly through a ramp and then settle at a new operating point, as shown by the simulations. Another difference is the use of a hybrid system (BESS and SESS) that operate mutually cooperating, changing their reference powers gradually, avoiding transients in the power injected by the wind turbine into the grid.

For future work, a program based on artificial intelligence, fuzzy logic or other control logic could be developed to manage all the reference power signals of the wind turbines. So that the sum of the power of all of them is equal to the requested output power for the wind power plant. This is because the state of charge of each HESS connected to each wind turbine is different, resulting in different operating points for each wind turbine. It would be beneficial to consider integrating pitch angle control into the HESS state-of-charge management algorithm. Instead of using the optimal angle, it may be preferable to set a different angle $(\text{e.g.}, \beta = 4^{\circ})$ to store or supply mechanical energy when the system requires it. This improves the ability of the energy storage system to adapt to changes in wind speed, thus maintaining constant

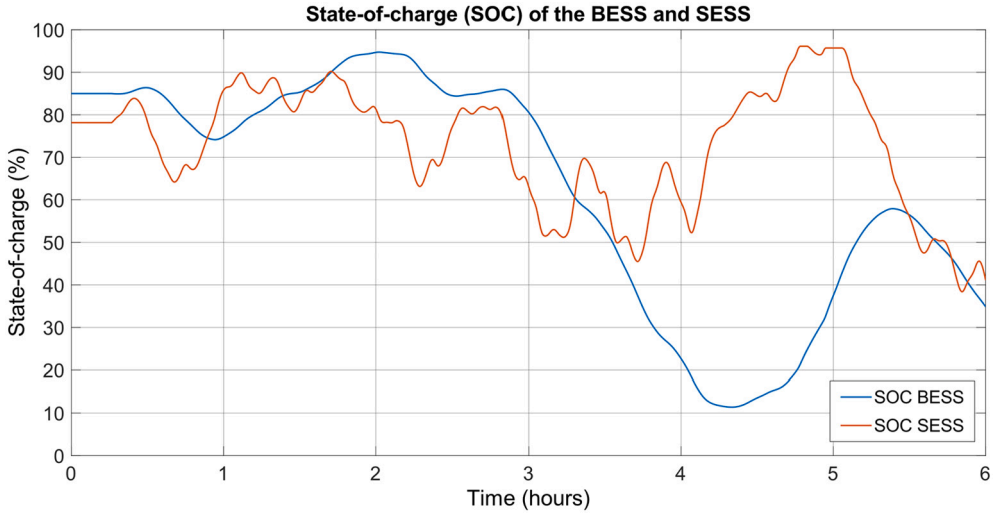

Fig. 36. State of charge of the BESS and SESS with WS3.

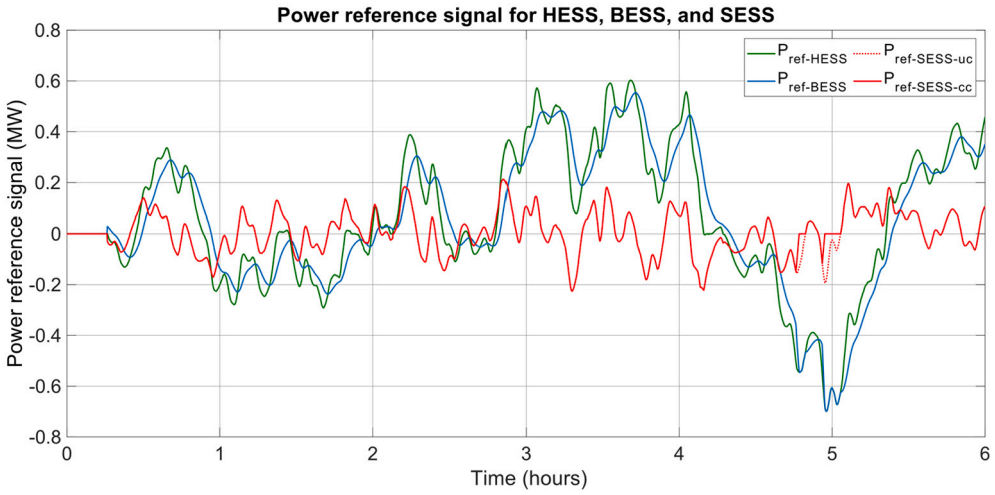

Fig. 37. Reference power signals for HESS, BESS and SESS with WS3.

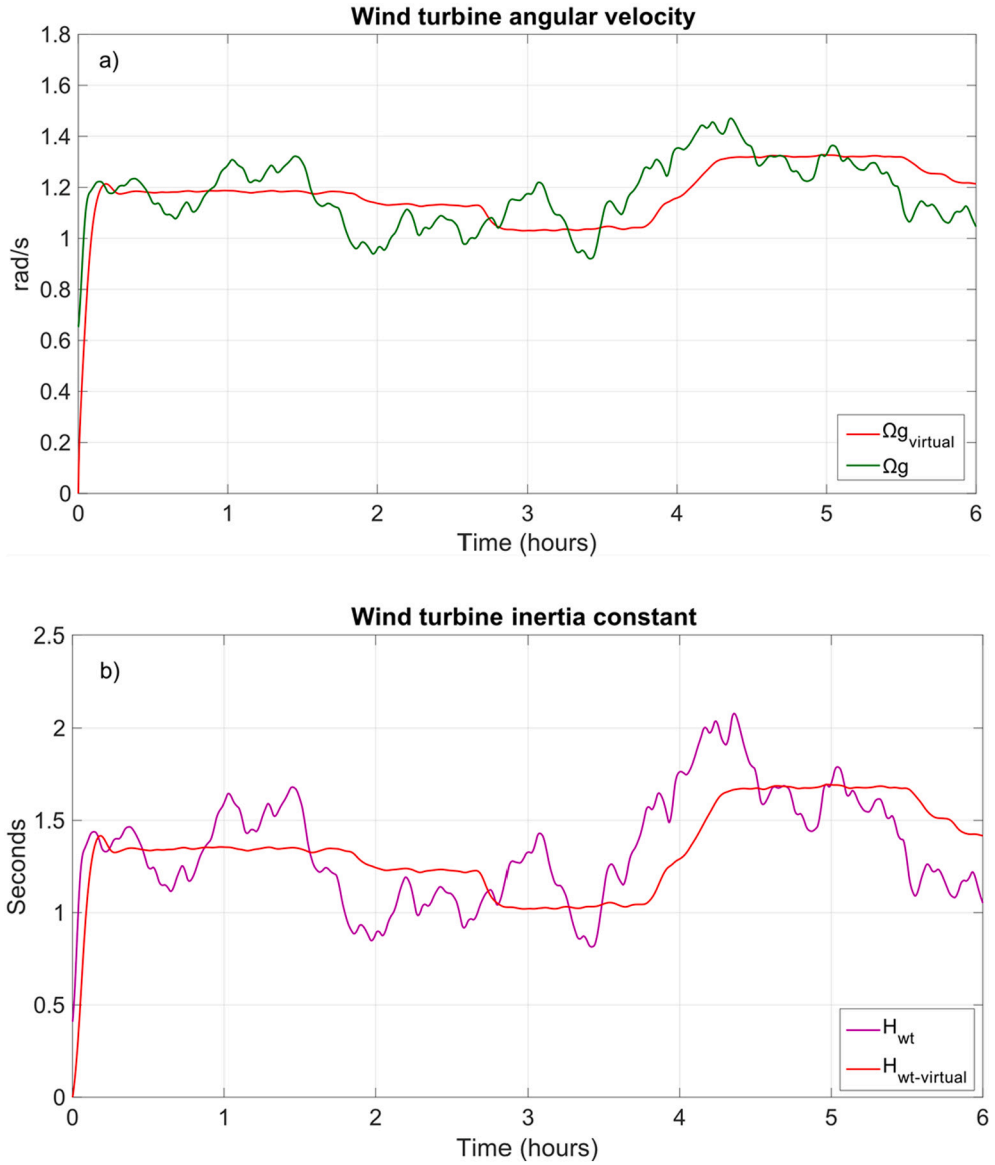

Fig. 38. (a) Angular velocity of the wind turbine observed from the generator side (Ω_g) and angular velocity of the wind turbine observed from the grid side ($\Omega_{g\_virtual}$) and (b) The variable inertia constant of the wind turbine (H_{wt}) and the inertia constant observed from the grid side ($H_{wt\_virtual}$).

power for much longer.

Thanks to the technological development of energy storage systems, wind energy will be able to achieve significantly higher penetration levels in power grids. Therefore, it will be one of the key renewable energy sources for the transition to a modern, sustainable, and CO_2-free power system.

Funding

This research received no external funding.

Declaration of competing interest

The authors declare that they have no known competing financial interests or personal relationships that could have appeared to influence the work reported in this paper.

Data availability

Data will be made available on request.

Acknowledgments

I would like to thank the support provided by the Polytechnic University of Catalonia. I would also like to thank Dr. José Luis Romeral Martínez for advising me in the development of this project.

Appendix A

Table A.1
Wind turbine parameters.

Description	Symbol	Value	Unit
Blade radius	R	50	m
Air density	ρ	1.225	$kg.m^2$
Aerodynamic constants	$(c_1, c_2, c_3, \ldots. c_9)$	(0.73, 148, 0.58, 0.002, 2.14, 13, 18.5, 0.002, 0,003)	–
Optimal power coefficient	C_{p_opt}	0.435	–
Optimal tip-speed ratio	λ_{opt}	7.199	rad
Optimal constant	k_{opt}	7.8246×10^5	$kg.m/rad^2$
Moment of inertia of the wind turbine	J_t	6.10^6	$kg.m^2$

Table A.2
DD-PMSG generator parameters.

Description	Symbol	Value	Unit
Rated active power	P_s	2.5	MW
Stator voltage rating (L-L)	V_n	690	V
Number of pole pairs	p	42	–
Nominal rotational speed	Ω_n	14.5	rpm
Stator resistance	r_s	4.23	mΩ
Stator inductance d axis	L_d	0.322	mH
Stator inductance q axis	L_q	0.322	mH
Magnetic flux	ϕ	9.1	Wb
Moment of inertia of the generator	J_g	$4.2.10^4$	$kg.m^2$

Table A.3
BESS DC/DC converter parameters.

Description	Symbol	Value	Unit
Inductance	L_{p_BESS}	13.8	mH
Low voltage side capacitance	C_{LVS_BESS}	51	μF
High voltage side capacitance	C_{HVS_BESS}	15	mF

Table A.4
SESS DC/DC converter parameters.

Description	Symbol	Value	Unit
Inductance	L_{p_SESS}	13.8	mH
Low voltage side capacitance	C_{LVS_SESS}	256	μF
High voltage side capacitance	C_{HVS_SESS}	10	mF

References

[1] Renewables 2021 Global Status Report (REN21), Available online, https://www.ren21.net/wp-content/uploads/2019/05/GSR2021_Full_Report.pdf. (Accessed 18 February 2022).

[2] I.A. Nassar, I.M. Kassem, M.N. Ali, Influence of using intermittent renewable energy sources on the power system operation, in: 21st International Middle East Power Systems Conference (MEPCON), Cairo, Egypt, 17-19 December, 2019, https://doi.org/10.1109/MEPCON47431.2019.9008222.

[3] A. Sajadi, L. Strezoski, V. Strezoski, M. Prica, K.A. Loparo, Integration of renewable energy systems and challenges for dynamics, control, and automation of electrical power systems, WIREsEnergy Environ (2019) 8, https://doi.org/10.1002/wene.321.

[4] S.D. Ahmed, F.S.M. Al-Ismail, M. Shafiullah, F.A. Al-Sulaiman, I.M. El-Amin, Grid integration challenges of wind energy: a review, in: IEEE Access: Practical Innovations, Open Solutions 8, 2020, pp. 10857–10878, https://doi.org/10.1109/access.2020.2964896.

[5] H. Zhao, Q. Wu, S. Hu, H. Xu, C.N. Rasmussen, Review of energy storage system for wind power integration support, Appl. Energy 137 (2015) 545–553, https://doi.org/10.1016/j.apenergy.2014.04.103.

[6] K. Shivarama Krishna, K. Sathish Kumar, A review on hybrid renewable energy systems, Renew. Sust. Energ. Rev. 52 (2015) 907–916, https://doi.org/10.1016/j.rser.2015.07.187.

[7] S. Koohi-Fayegh, M.A. Rosen, A review of energy storage types, applications and recent developments, J. Energy Storage 27 (101047) (2020), 101047, https://doi.org/10.1016/j.est.2019.101047.

[8] P.H.A. Barra, W.C. de Carvalho, T.S. Menezes, R.A.S. Fernandes, D.V. Coury, A review on wind power smoothing using high-power energy storage systems, Renew. Sust. Energ. Rev. 137 (2021), 110455, https://doi.org/10.1016/j.rser.2020.110455.

[9] M. Jabir, H. Azil Illias, S. Raza, H. Mokhlis, Intermittent smoothing approaches for wind power output: a review, Energies 10 (2017) 1572, https://doi.org/10.3390/en10101572.

[10] G. Ren, J. Liu, J. Wan, Y. Guo, D. Yu, Overview of wind power intermittency: impacts, measurements, and mitigation solutions, Appl. Energy 204 (2017) 47–65, https://doi.org/10.1016/j.apenergy.2017.06.098.

[11] L. Qu, W. Qiao, Constant power control of DFIG wind turbines with supercapacitor energy storage, IEEE Trans. Ind. Appl. 47 (2011) 359–367, https://doi.org/10.1109/tia.2010.2090932.

[12] F. Díaz-González, A. Sumper, O. Gomis-Bellmunt, F.D. Bianchi, Energy management of flywheel-based energy storage device for wind power smoothing, Appl. Energy 110 (2013) 207–219, https://doi.org/10.1016/j.apenergy.2013.04.029.

[13] L. Barelli, D.-A. Ciupageanu, A. Ottaviano, D. Pelosi, G. Lazaroiu, Stochastic power management strategy for hybrid energy storage systems to enhance large scale wind energy integration, J. Energy Storage 31 (2020), 101650, https://doi.org/10.1016/j.est.2020.101650.

[14] N. Ben Halima, A. Oualha, Management of energy produced by a wind turbine connected to the network in order to inject a constant power, in: 2016 17th International Conference on Sciences and Techniques of Automatic Control and Computer Engineering (STA), 2016, pp. 640–645.

[15] Y. Ou, J. Wen, L. Wang, Z. Yu, J. Huang, Q. Ai, L. Fen, A novel control strategy of super capacitor-battery energy storage system, in: 2015 5th International Conference on Electric Utility Deregulation and Restructuring and Power Technologies (DRPT), 2015, pp. 2089–2093, https://doi.org/10.1109/DRPT.2015.7432591.

[16] R. Poudel, V. Krishnan, J. Reilly, P. Koralewicz, I. Baring-Gould, Integration of storage in the DC link of a full converter-based distributed wind turbine, IEEE Power & Energy Society General Meeting (PESGM) 2021 (2021) 1–5, https://doi.org/10.1109/PESGM46819.2021.9638225.

[17] T. Ackermann, in: Wind Power in Power Systems, 2nd ed., John Wiley & Sons: The Atrium, Chichester, England, 2005, pp. 562–563.

[18] H. Matayoshi, A.M. Howlader, M. Datta, T. Senjyu, Control strategy of PMSG based wind energy conversion system under strong wind conditions, Energy Sustain. Dev. 45 (2018) 211–218, https://doi.org/10.1016/j.esd.2018.07.001.

[19] P. Gajewski, K. Pieńkowski, Advanced control of direct-driven PMSG generator in wind turbine system, Arch. Electr. Eng. 65 (2016) 643–656, https://doi.org/10.1515/aee-2016-0045.

[20] B. Wu, Y. Lang, N. Zargari, S. Kouro, in: Power conversion and control of wind energy systems, 1st ed., John Wiley & Sons, Hoboken, New Jersey, United State, 2011, pp. 275–301.

[21] M.A. Abdullah, A.H.M. Yatim, C.W. Tan, R. Saidur, A review of maximum power point tracking algorithms for wind energy systems, Renew. Sust. Energ. Rev. 16 (5) (2012) 3220–3227, https://doi.org/10.1016/j.rser.2012.02.016.

[22] J. Pande, P. Nasikkar, K. Kotecha, V. Varadarajan, A review of maximum power point tracking algorithms for wind energy conversion systems, J. Mar. Sci. Eng. 9 (11) (2021) 1187, https://doi.org/10.3390/jmse9111187.

[23] S.A. Gorji, H.G. Sahebi, M. Ektesabi, A.B. Rad, Topologies and control schemes of bidirectional DC–DC power converters: an overview, in: IEEE Access: Practical Innovations, Open Solutions 7, 2019, pp. 117997–118019, https://doi.org/10.1109/access.2019.2937239.

[24] H. Zheng, S. Li, C. Zang, W. Zheng, Coordinated control for grid integration of PV array, battery storage, and supercapacitor, in: 2013 IEEE Power & Energy Society General Meeting, Vancouver, Canada, 21-25 July, 2013, https://doi.org/10.1109/PESMG.2013.6672725.

[25] J. Chaires, H.B. Karayaka, Y. Yan, P. Gardner, Solar farm hourly dispatching using super-capacitor and battery system, in: 2016 Clemson University Power Systems Conference (PSC), Clemson, SC, 8-11 March, 2016, https://doi.org/10.1109/PSC.2016.7462867.

[26] F. Díaz-González, O. Gomis-Bellmunt, A. Sumper, Energy Storage in Power Systems, in: 1st ed.;, John Wiley & Sons: The Atrium, Chichester, United Kingdom, 2016, pp. 163–207.